The Making Of the DRAKKAR FORCING SET DFS5

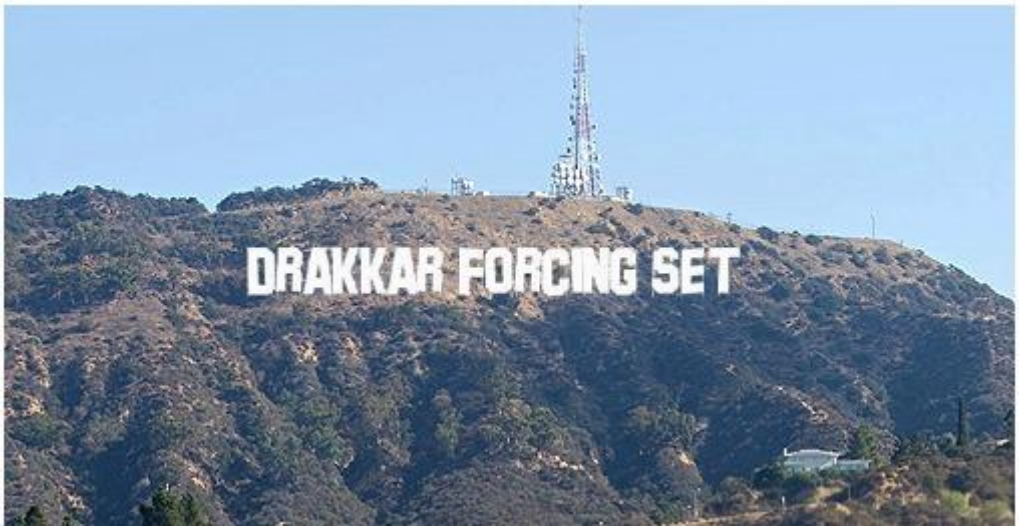

Raphael Dussin[*], Bernard Barnier, Laurent Brodeau[**], and Jean Marc Molines

MultiscalE Ocean Modelling (MEOM) Team
Laboratoire de Glaciologie et Géophysique de l'Environnement
CNRS, Université de Grenoble, OSUG, Grenoble, France

[*]*Now at Institute of Marine and Coastal Sciences, Rutgers University, New Brunswick,USA*

[**]*Department of Meteorology, Stockholm University, Stockholm, Sweden*

Contact Email
bernard.barnier@lgge.obs.ujf-.grenoble.fr

DRAKKAR/MyOcean Report 01-04-16

DRAFT
April 2016

Table of content

1 INTRODUCTION

Simulating the evolution of the global ocean over the last few decades using Ocean General Circulation models (OGCMs) has been made possible since globally gridded inter-annual weather reanalysis products have become available. Atmospheric fields from these reanalyzes are used to estimate fluxes to be applied as surface boundary conditions for OGCMs. In this context, DRAKKAR[1] is using atmospheric reanalyses carried out at the European Centre for Medium Range Weather Forecast (ECMWF) to develop data sets (referred to as the Drakkar Forcing Sets, DFS) intended to drive ocean hindcasts simulations of the last five decades (1958 to present). DRAKKAR produced several forcing data sets based on the ERA40 reanalysis and ECMWF real-time analyses (see Brodeau et al., 2010). Widely used, these data sets (DFS3 and DFS4, see Annex) provide the surface meteorological variables required as input by the NEMO-based hierarchy of model configurations to calculate the air-sea fluxes that drive hindcasts simulations. The present report describes the making of the latest forcing set, the DFS5, mainly based on the recent reanalysis ERA-interim (ERAi hereafter).

This report is organised as follows.

- Section 2 presents a summary of the main characteristics of DFS5.2. This includes a short description of the corrections applied to ERAi for the period 1979-2010 and exposes how DFS5.2 is extended backward in time from 1979 until 1958 using ERAi and ERA40, to finally achieve the final DFS5.2 forcing set for the period 1958 to 2010 (extended to 2015 in February 2016).
- Section 3 describes in details the corrections applied to ERAi over the period 1979-2010.
- Section 4 describes the extention of DFS5.2 to 1958-1978 on the basis of ERA40.
- Section 5 illustrates the effects of the corrections by comparing the forcing variables of DFS5.2 with those of the original ERAi.
- Section 6 presents a brief assessment of DFS5.2 from model hindcast simulations carried out with the Drakkar hierarchy of NEMO configurations and raised a few issues regarding the use of DFS5.2.
- Finally, two sections describe in details the various stages that contributed to the definition of the corrections applied to the original ERAi. Section 7 provides a short assessment of the original ERAi as a forcing of an ocean model. Section 8 provides a brief description of the previous DFS3 and DFS4.

2 DESCRIPTION OF DFS5.2

This section briefly recalls the main characteristics of the Drakkar Forcing Set 5.2 that has been developed to drive ocean hindcasts of the period 1958 to 2015 (see also Table 1). It includes the following surface variables required by the NEMO bulk formula to calculate heat, freshwater and momentum fluxes across the air-sea interface (i.e. the surface boundary condition to the model primitive equations).

- zonal and meridional components of the 10-m wind : *u10, v10*

[1] *DRAKKAR (http://www.drakkar-ocean.eu/) is a scientific and technical coordination between French research teams (LEGI-Grenoble, LPO-Brest, LOCEAN-Paris), MERCATOR-ocean, NOC Southampton, IFM-Geomar Kiel, and other teams in Europe and Canada. We propose to design, carry out, assess, and distribute high-resolution global ocean/sea-ice numerical simulations based on the NEMO platform (www.nemo-ocean.eu) performed over long periods (five decades or more), and to improve and maintain a hierarchy of state-of-the-art ocean/sea-ice model configurations for operational and research applications.*

- 2-m air humidity : *q2*
- 2-m air temperature : *t2*
- downward shortwave radiation at the sea surface : *radsw*
- downward longwave radiation at the sea surface : *radlw*
- precipitation total and solid : *P, snow*

The DFS5.2 data set has been built to take advantage of ERA-interim, the most recent atmospheric reanalysis produced at ECMWF (Dee et al., 2011). ERAi provides the surface atmospheric variables required to drive global ocean hindcasts simulations for the period 1979-2015. Compared to previous reanalyses, it has the advantage of an increased spatial resolution (~0.7°) and denser time sampling (3 hours) that resolves the diurnal cycle. However, ERAi is limited to the period 1979-2015, and has to be combined to another data set, e.g. ERA40 which does include the period 1958-1978. DFS5.2 has been constructed following a step by step methodology described below.

2.1 Summary of the Methodology

At the time of the making of DFS5.2, ERAi was available only for the period 1979 to 2010 so the processing described below is relative to that period. The process has been applied to years 2011 to 2015 after they were available.
The frequency of DFS5.2 over this period is 3 hourly for wind, air temperature and humidity, and daily for radiation and precipitation (an analytical diurnal forcing can be used for the solar flux in NEMO if desired). The spatial resolution is nearly 0.7°.

2.1.1 Step 1: Assessment of ERAi forcing variables.

ERAi surface variables have been (i) compared to other products and (ii) used to drive global ocean hindcasts over the period 1979-2010 with the ORCA025[2] configurations. This preliminary work guided the needs for corrections. The main conclusions of this assessment are that corrections are needed for downward radiation, wind speed and precipitation is the inter-tropical band, and that the surface air temperature and humidity are too high at polar latitudes. The analysis pointed out the existence of discontinuities in the Precipitation fields that needed to be removed. A detailed description of this assessment is presented in Section 7.

2.1.2 Step 2: Corrections to ERAi forcing variables for the period 1979-2010

Following the conclusions of step 1, a first set of corrections has been applied to ERAi atmospheric surface variables.

- Radiations have been corrected by comparison to the GEWEX radiation fluxes (Pinker and Laszlo, 1995).

- The wind speed has been corrected (i.e. increased) in the inter-tropical band by comparison to the Qscat wind climatology.

- Air temperature and humidity have been corrected (i.e. cooled and dried) in the Arctic according to the POLES climatology (Rigor et al., 2000), and in the southern ocean near the Antarctic continent according to a downscaling of ERA40 with a regional model (Mathiot et al., 2010). The cooling/drying of t2/q2 in the Southern ocean corresponds is a linear decrease of 0.13°C per degree latitude that starts at 60°S (and reaches 2°C at 75°S).

- Correction of the liquid precipitation fields to remove unrealistic time discontinuities (induced by changes in the nature of assimilated observations) and to correct for excessive

[2] *ORCA025 is the eddy-permitting, 1/4° resolution, global configuration of the Drakkar hierarchy of models (Barnier et al., 2006).*

precipitation in the inter-tropical band, following the approach proposed by Storto et al. (2012).
- Final adjustment of the radiation fluxes to re-equilibrate the global heat balance.

The above corrections are fully described in Section 3.

2.1.3 Step 3: Extension of DFS5.2 to the period 1958-1978

DFS5.2 is extended backward in time until 1958 using the ERA40 reanalysis. The methodology uses the 23 year period common to both data sets (1979-2001) to match ERA40 fluxes to those of DFS5.2 in a continuous way.
Radiation (shortwave and longwave downward radiation) and ttotal precipitation (rain and snow) are the daily climatology of DFS5.2 (period 1979-2010). This was also the strategy for DFS4 and for CORE.
The backward extension of the surface atmospheric variables required for the calculation of turbulent fluxes (t2, q2, u10 and v10) makes use of the ERA40 reanalysis in the following way.

The 3-hourly "*synoptic scales*" of ERA40 of the period 1958-1978 are calculated as the difference between instantaneous original ERA40 fields and the ERA40 daily mean climatology (period 1958-1978). Linear trends are calculated and removed. The daily climatology of DFS5.2 (period 1979-2010) is then added to the ERA40 synoptic scales to give the instantaneous DFS5.2 fields. A consequence is that the variables in DFS5.2 show no trends over the period 1958-1978 and that the climatological mean of that period is the same as for the period 1979-2010.

To provide a homogeneous record, all fields are provided on a 0.7° grid, every 3h for the turbulent variables and daily for radiation and precipitation. The whole process is described in details in Section 4.

2.1.4 Step 4: Period 2011-2015.

The extension of DFS5.2 over the recent period 2011 to 2015 applies the same processing already used for the period 1979-2010 to ERAi. Note that the offset between the 1979-2010 mean and the 2011-2015 mean has been corrected.

Table 1: Major characteristics of the DFS5.2 forcing data set.

<table>
<tr><th rowspan="2">Variable name</th><th rowspan="2">Description</th><th rowspan="2">Units</th><th colspan="2">DFS5.1 Origin, time and grid resolution</th></tr>
<tr><th>1958-1978</th><th>1979-2015</th></tr>
<tr><td>u10</td><td>Zonal wind speed at 10 m height</td><td>$m.s^{-1}$</td><td rowspan="4">ERAi* daily climatology (1979-2010) combined with ERA40** 3-hourly synoptic scales (1958-1978) 0.7° resolution</td><td rowspan="4">ERAi* 3-hourly 0.7° resolution</td></tr>
<tr><td>v10</td><td>Meridional wind speed at 10 m height</td><td>$m.s^{-1}$</td></tr>
<tr><td>t2</td><td>Air temperature at 2 m height</td><td>°C</td></tr>
<tr><td>q2</td><td>Air specific humidity at 2 m height</td><td>kg/kg</td></tr>
<tr><td>radsw</td><td>Downward shortwave radiation</td><td>$W.m^{-2}$</td><td rowspan="2">ERAi* daily climatology (1979-2010) 0.7° resolution</td><td rowspan="2">ERA-interim daily 0.7° resolution</td></tr>
<tr><td>radlw</td><td>Downward longwave radiation</td><td>$W.m^{-2}$</td></tr>
<tr><td>P</td><td>Total precipitation</td><td>mm/day</td><td rowspan="2">ERAi* daily climatology 0.7° resolution</td><td rowspan="2">ERA-interim daily 0.7° resolution</td></tr>
<tr><td>snow</td><td>Snow fall</td><td>mm/day</td></tr>
<tr><td colspan="5">* ERAi* = ERA-interim variables after implementation of the corrections described in Section 3.
** ERA40 resolution is 6-hourly and 1.125°. To provide a homogeneous record, ERA40 have been interpolated at the resolution of ERAi (3-hourly and 0.7°).</td></tr>
</table>

2.2 Global budgets of heat and freshwater of the various DFS

Work in progress to provide a Table with global heat and freshwater budgets for all DFS forcing.

3 CORRECTIONS TO ERAi FOR THE PERIOD 1979-2010

This section describes the modifications applied to the ERAi surface variables that yielded the DFS5.2 forcing sets for the period 1979-2010 (later extended to 2015). We explain how we have corrected t2 & q2 in the Arctic and in the Southern ocean. The resulting improvements in the representation of the sea-ice obtained in a coarse resolution model are then assessed. This modification is very local and does not affect much the global balances. Then, we discuss more precisely the method used to increase the wind strength, which has significant consequences on the heat and freshwater budgets (-3.77 $W.m^{-2}$ and -3.83 mm/day). Corrections of radiation fluxes are then described. The effects of those corrections on the global heat balance are -3.8 $W.m^{-2}$, which is important if compared to the net heat flux associated to global warming (which estimates vary around +0.5 W/m^2) but is still within the error bar of air-sea fluxes estimates. Corrections applied to precipitation are described. This has been a difficult task since the constraint of preserving a closed freshwater budget had to be satisfied while applying those spatial corrections. The results of coarse-resolution model (ORCA2) sensitivity simulations are sometimes used to provide assessments of the effects of the corrections.

3.1 Air temperature and humidity in the Arctic and Southern Oceans

Arctic:

Given that the ECMWF reanalysis ERAi is much warmer/moister than DFS4.3 in the Arctic (Fig. 1), we apply similar corrections on air temperature and humidity at 2 meters than those proposed by Brodeau et al. (2010). Those corrections are based on the POLES monthly climatology for air temperature (http://iabp.apl.washington.edu/data_satemp.html). They are applied only over sea-ice-covered regions, using a monthly climatology of ice-fraction based on SSM/I satellite data. The POLES air temperature and SSM/I ice-cover climatologies (period 1979-1998) have been used. The method then consists in computing a climatological monthly offset of air temperature between the atmospheric reanalysis and POLES observations. Then a correction based on this offset is applied to the high-frequency fields. Corrections reduce the mean air temperature by more than 0.6°C everywhere in the Arctic except in the Baffin Bay where it is slightly less. The strongest correction is applied above the Laptev Sea, the Lincoln Sea and close to the North Pole along the Beaufort gyre. Regions where the mean correction is particularly important are also found over the Barents Sea and the Greenland Sea but on smaller length scales. The effect of this correction on ERAi 2 m air temperature t2 is shown in Fig. 2.

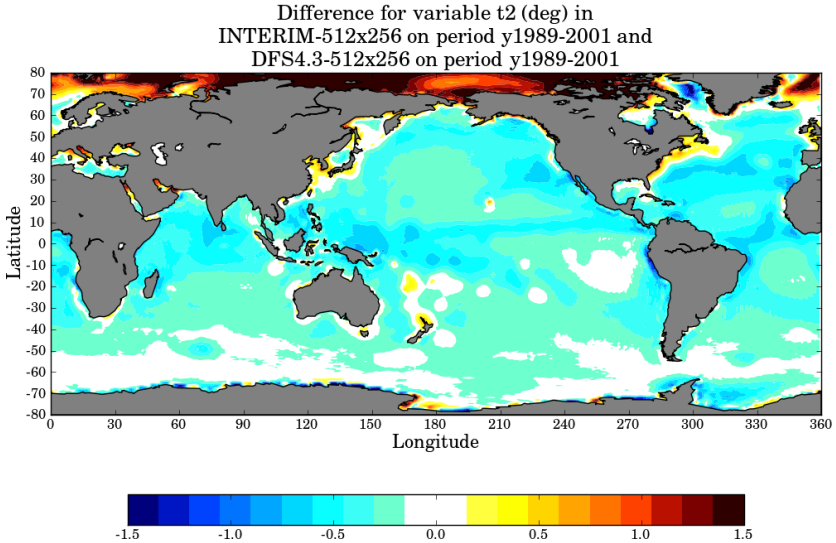

Figure 1. Difference in air temperature between ERAi and DFS4.3 (1989-2001 mean). Units are °C.

Figures 2&3 show the sea-ice area and extent in respectively March and September in two ORCA246 (2° and 46 vertical levels) simulations compared to observations from NSIDC (blue curves). The reference ORCA246 simulation (forced by the original ERAi) is shown with red curves and the corrected ERAi (with only air temperature and humidity corrections in the arctic) is shown with black curves. It appears that the reduction of air temperature gives an overestimation of ice area in winter but a better extent. In summer, there is a major improvement of both ice area and extent. As this modification was already applied to ERA-40 in order to build DFS4.3, it was relevant to reproduce it on ERAi to build DFS5. These modifications give good results on sea-ice properties and have a very minor impact of global net heat flux.

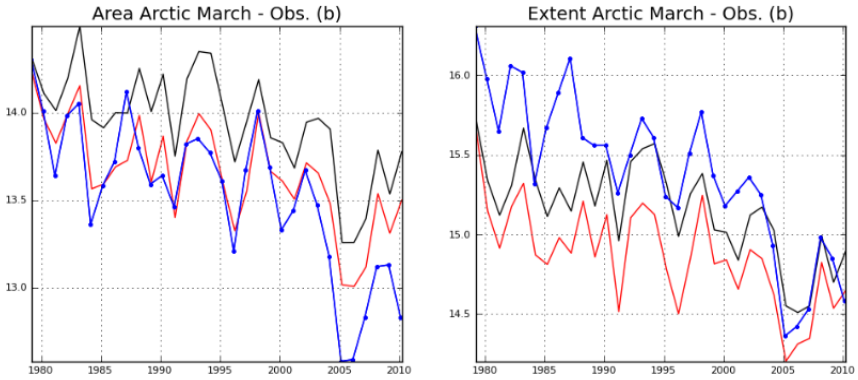

Figure 2. Ice area and extent in March in two ORCA246 simulations forced by the original ERAi (red) and the corrected-ERAi (black). Blue curves are observations from NSIDC. Units are in 10^6 km^2.

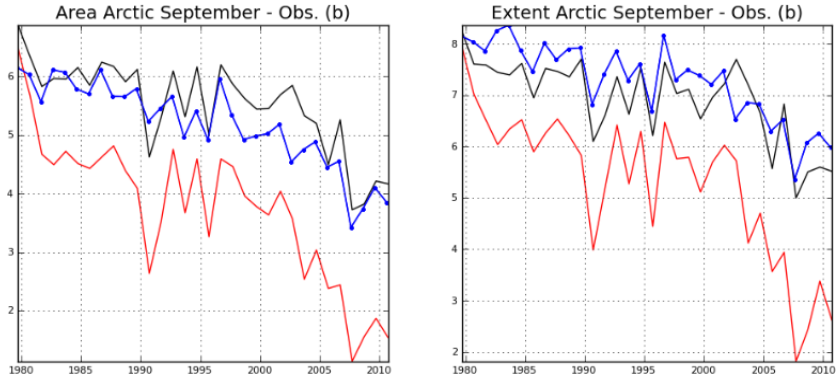

Figure 3. Ice area and extent in September in two ORCA246 simulations forced by the original ERAi (red) and the corrected-ERAi (black). Blue curves are observations from NSIDC. Units are in 10^6 km^2.

Southern Ocean:

ERAi air temperature is found to present an important warm bias over the whole Antarctic continent (more than a few °C, Fréville et al., 2014). The comparison of ERAi and ERA40 near surface temperatures (after application of an orographic correction) with those measured at the coastal weather stations around Antarctica (Bracegirdle and Marshall, 2012) suggests a more contrasted picture. Most stations exhibit only a small bias (<2°C) or no significant bias, and very few a small negative bias. The picture is almost identical for ERA40 and ERAi. Mathiot et al (2012) found that ERA40 2m air temperature was ~2°C warmer in average along the coast of the Antarctic continent than that produced by donwscaling performed with a regional atmospheric model that compared well to weather station observations. They suggest that ERA40 should be corrected from that bias.

Based on these studies, we have decided to apply a cooling (and associated drying) correction of the ERAi 2m air temperature (and specific humidity). The cooling of 0.13°C per degree of latitude is applied between 60°S and 75°S and yields a 2°C cooling at 75°S (Fig. 4).

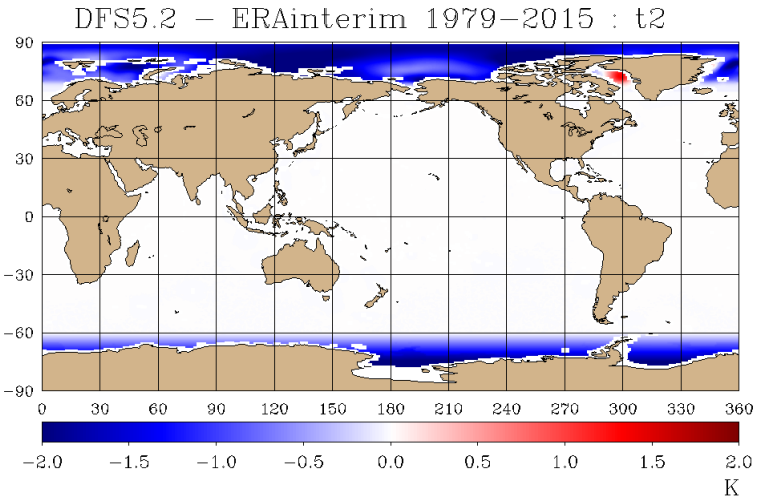

Figure 4: Mean (1979-2015) 2 m air temperature difference between DFS5.2 and ERAi. In the Arctic the difference is due to the correction to the POLE climatology. In the Southern Ocean, the difference is due to the poleward linear decrease of t2 starting at 60°S.

3.2 Wind speed

ERAi forced simulations have shown to have weak gyre circulation. Other independent studies (e.g. Meinvielle et al., 2013) suggest that ERAi winds are underestimated in the inter-tropical band (30°S-30°N). This is also suggested by Figure 5 which compares the zonal mean of wind module (time-averaged over the period 2000-2006) in ERAi, DFS4.3 and QuikSCAT. ERAi have weaker values than QuikSCAT almost everywhere. The greatest discrepancies are found between 40°S and 40°N, and can be as large as 0.8 m/s at the equator. In DFS4.3, ERA-40 winds have been rescaled towards QuikSCAT so values are obviously closer but still a little bit less intense than QuikSCAT.

Therefore, we decided to strengthen ERAi winds by adding a constant in time background value to the mean wind, the amplitude of which is estimated from the QuikSCAT/ERAi mean wind module ratio. As explained below, this solution has been chosen instead of straightforward multiplication by such ratio of the wind components because it yields a lower increase of evaporation.

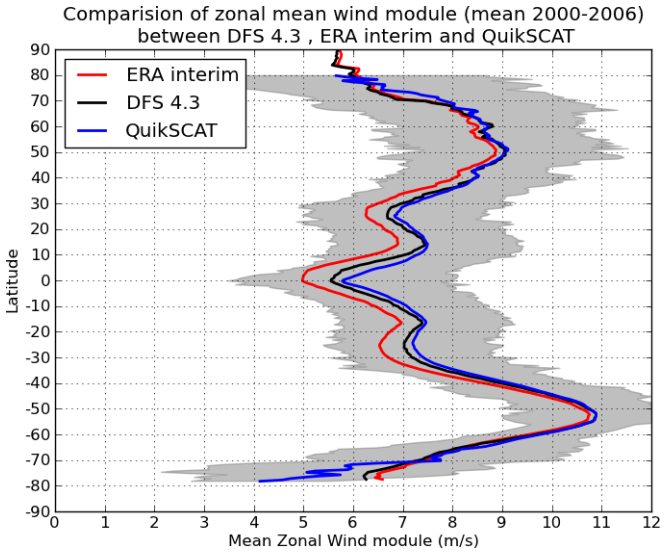

*Figure 5. Zonal average of the mean (2000-2006) 10 m wind speed. In **red** the original ERAi wind speed. In **blue** QuickSCAT wind speed estimate and its spread is shown by the grey shading. In **black** the wind from DFS4.3, i.e. the ERA40 corrected with QuickSCAT winds.*

Let us define α as the local (i.e. defined at every grid point) ratio of QuikSCAT over ERAi wind module in the formula below:

$$\alpha = \frac{\frac{1}{T}\sum_i U^i_{QuikSCAT}}{\frac{1}{T}\sum_i U^i_{ERAi}}$$

where T is the 2000-2008 period, i is the time-step and U is the wind module defined as:

$$U = \sqrt{u_{10}^2 + v_{10}^2}$$

The α ratio obtained by a straight calculation is somewhat noisy. A smooth ratio α_{sm} is calculated by filtering α with an anisotropic box filter. The box size is 14 grid points along the meridional direction and 28 grid points along the zonal direction, which corresponds to a 10° by 20° box. The maximum correction allowed is 15% and there is no correction above of 60°N and below of 60°S (a linear transition is done over 10 grid points, ~7° in latitude°). In practice, α_{sm} varies between 1 and 1.15 and shows small gradient to aviod any significant distortion of the divergence or the curl pattern (Figure 6). Wind speed increase is maximal at low latitudes and is also important in the Gulf Stream and the Kuroshio area. The correction brings a 0.5 to 1 Sv increase of the Florida-Bahamas transport in ORCA2 simulations, while being still very weak compared to observations due to the model viscosity. The eddy-permitting models are expected to show the similar behaviour but with changes of greater amplitude. No correction is applied beyond 60° latitude in both hemisphere, and only weak corrections are done south of 50°S. The methodology used does not have any impact on trends.

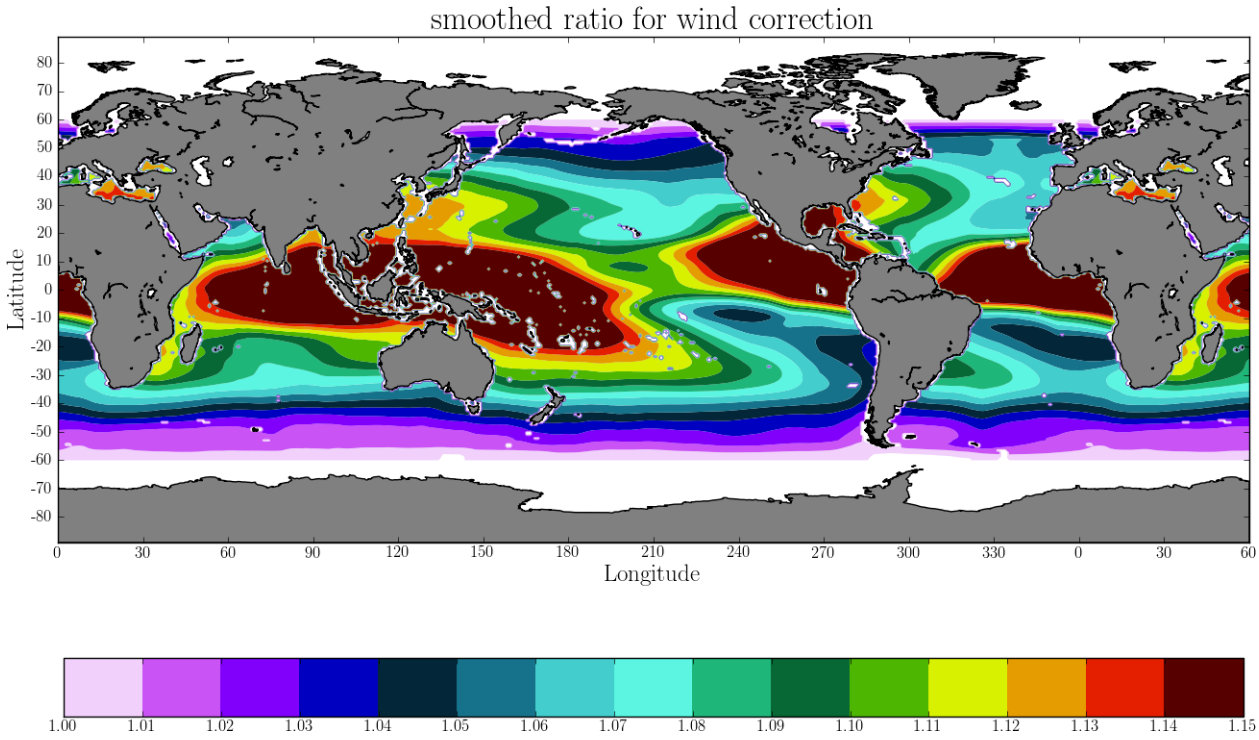

Figure 6. Multiplicative smoothed ratio α_{sm} used for wind speed enhancement.

Two different methods have been tested for the wind correction. The "multiplicative ratio" method in which the "corrected" wind speed (noted u^*_{10} hereafter) would be obtained by scaling the 10 m wind with the smooth ratio at every time-step:

$$u_{10}^{*} = \alpha_{sm} \times u_{10}$$
$$v_{10}^{*} = \alpha_{sm} \times v_{10}$$

The "background value" method (v2 hereafter) in which the smooth ratio is used to shift the mean without changing the variance of the field in the following way:

$$u_{10}^{*} = (\alpha_{sm} - 1) * \bar{u}_{10} + u_{10}$$
$$v_{10}^{*} = (\alpha_{sm} - 1) * \bar{v}_{10} + v_{10}$$

As an increase in wind speed leads to enhanced evaporation, the multiplication by a ratio gives wind increments proportional to the wind speed even in case of extreme events. This leads to much greater evaporation rates, which is something that we want to prevent since the ERAi freshwater budget is already unbalanced in favour of evaporation (by 3.3 mm/day). Note that the NCAR bulk formula used here might also be to blame for this excess of evaporation, since they significantly promote evaporation (compared to COARE for example, Brodeau et al. 2016, in preparation).

Figure 7 shows the difference of evaporation between the "multiplicative ratio" method (*v1*) and the "background value" method (*v2*). We clearly see that the *v2* method produces an evaporation increase of much smaller amplitude (up to 1 mm/day in the Gulf Stream). It gives an evaporation increase of 0.15 mm/day compared to the original ERAi, which is more acceptable than the 0.35 mm/day provided by the *v1* method (see Table 2), especially since this evaporation increase will have to be balanced by precipitations, already suspected as being overestimated in ERAi. Regarding the net heat flux, *v1* provides a dramatic cooling of the ocean whereas *v2* is much closer to balance. Since radiation fluxes will also be slightly reduced, the net heat flux in *v1* is certainly too low.

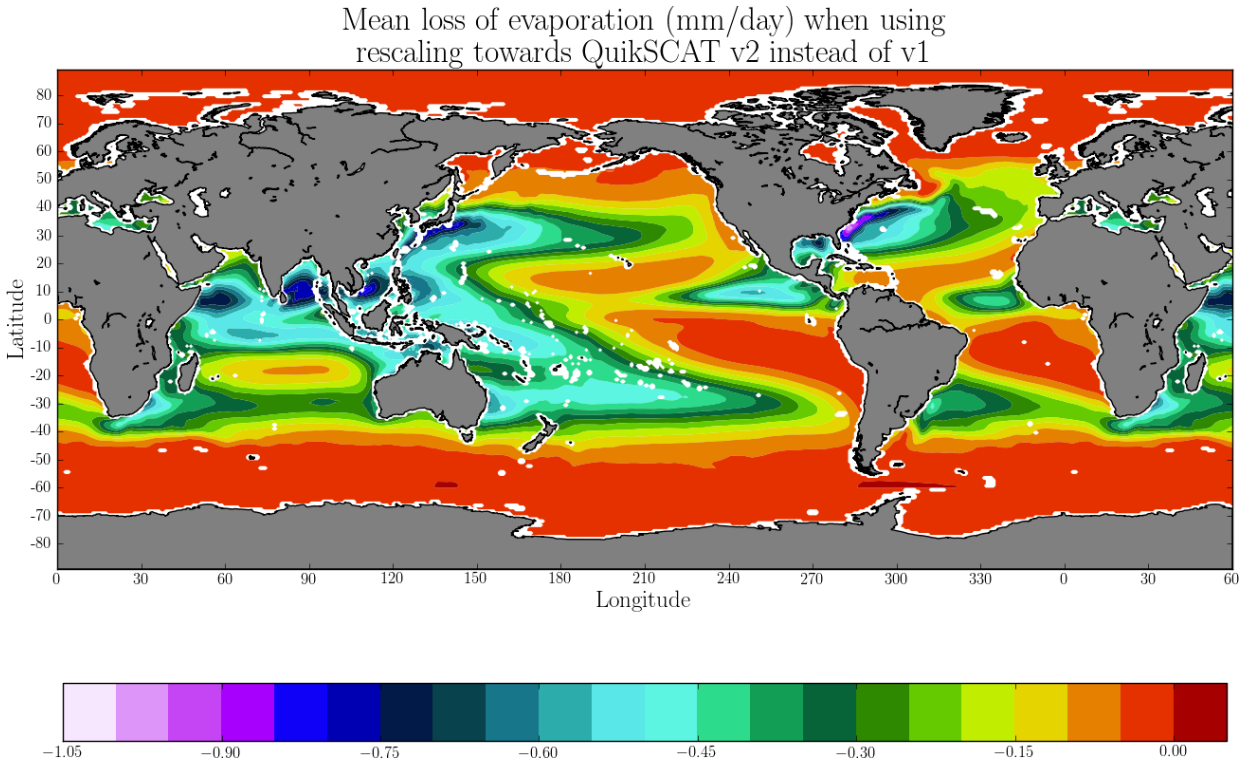

Figure 7. Differences in evaporation between the "background value" method (v2) and the "multiplicative ratio" method (v1). Negative values correspond to a diminution of evaporation in the background value method compared to multiplicative ratio method.

Table 2: Global mean evaporation and net heat flux (1979-2010 mean)

	Evaporation (mm/day)	Net Heat Flux ($W.m^{-2}$)
ERAi original	3.7	5.34
ERAi corrected by *v1*	4.05	-5.65
ERAi corrected by *v2*	3.85	0.83

3.3 Radiation fluxes

Achieving a good cloud cover representation in atmospheric model is a very tough task as it requires correctly resolved dynamics, as well as humidity and aerosols concentration in the air parcel. This cloud cover will then impact radiative transfer model which ultimately provide the downward shortwave and longwave radiation driving to the ocean model. Compared to satellite products (such as Gewex - Pinker and Laszlo, 1992 - or ISCCP), it appears that ERAinterim overestimates shortwave radiation and underestimates longwave radiation, the opposite behaviour of the two radiation fluxes being consistent with the existence of a flaw in cloud representation in ERAi that consists in a lack a cloud cover, thus leading to the observed biases in the radiation fluxes. Therefore it has been decided to reduce the shortwave radiation and increase slightly longwave radiation, using DFS4.3 (which is a corrected version of the ISCCP satellite data) as our reference.

Due to seasonality of the solar radiation at the poles, the only available method is obviously the multiplicative ratio method. We choose to correct the shortwave only in regions where the difference between ERAi and DFS4.3, averaged on the period 1984-2006, is greater than 10 $W.m^{-2}$. Longwave radiation is also corrected in regions where the difference between ERAi and DFS4.3, averaged on the period 1984-2006, is less than -2.5 $W.m^{-2}$.

The local ratios of ERAi radiation over DFS4.3 radiation have calculated for both shortwave and longwave radiation. Ratios are spatially smoothed using a Gaussian filter after application of "drowning" process (i.e. extrapolation of ocean values into land) to avoid the contamination of ocean values by land value during the smoothing. A masking is applied to remove correction at high latitudes and in closed seas (Hudson Bay, Mediterranean and Red seas, Persian Gulf,...). Finally, corrected fields are obtained by simple multiplication of every daily ERAi radiation field by those ratios, which are shown in figures 8&9.

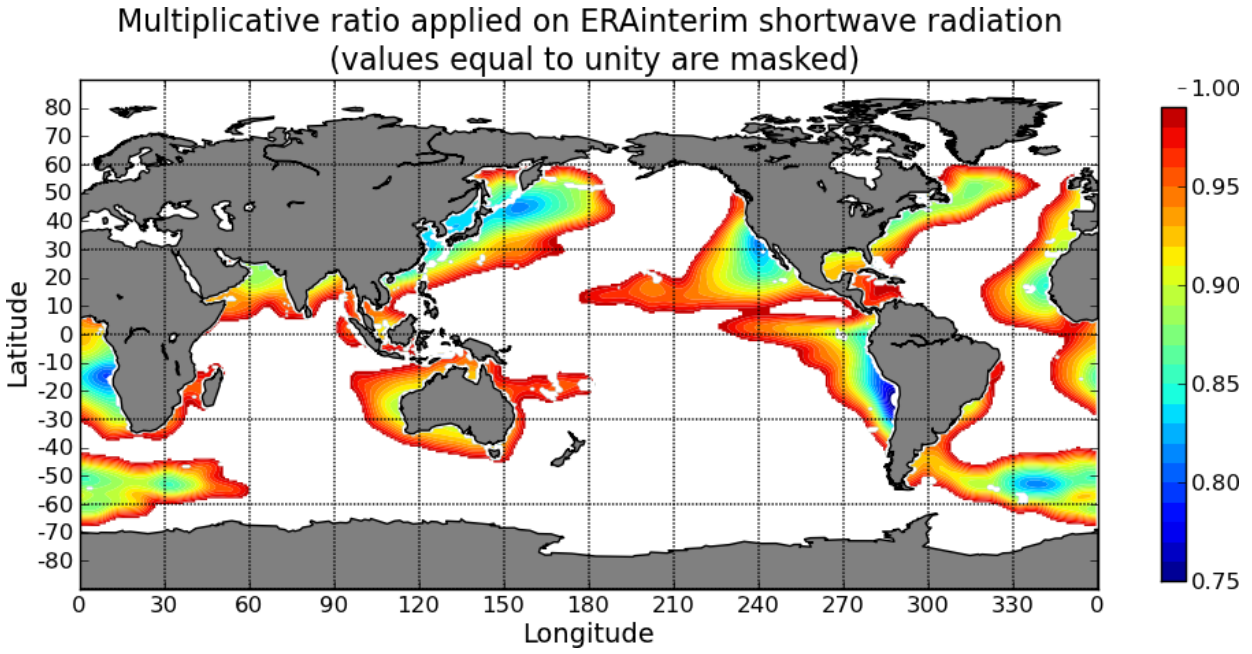

Figure 8. Multiplicative ratio applied to ERAi shortwave radiation

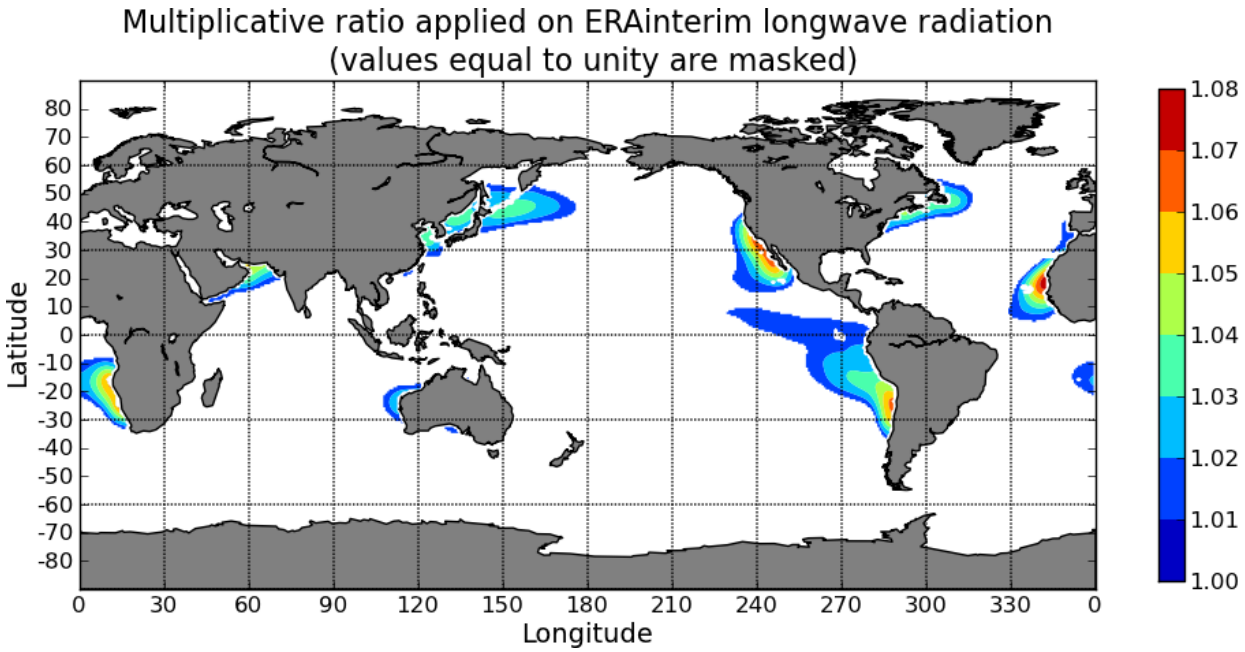

Figure 9. Multiplicative ratio applied to ERAi longwave radiation.

The effect of the corrections on the ERAi radiation fields are discussed in Section 4.

3.4 Precipitations

Regarding precipitations, various modifications have been performed. Linear trends have been removed and the corrections proposed by Storto et al. (2012) have been applied on the de-trended fields. The detrending process was motivated by the inaccuracy of precipitation trend in ERAi compared to the GPCP satellite product. Figure 10, adapted from Dee et al. (2011), shows that the precipitation trends in ERAi are not comparable to observations and these authors suggest it might be due to the variational bias correction.

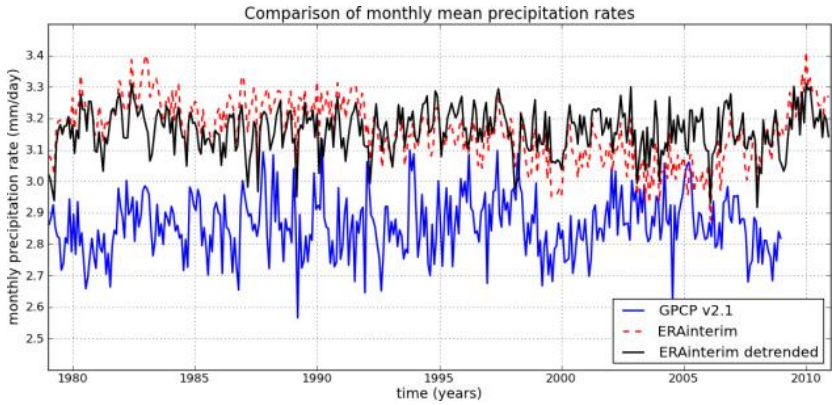

Figure 10. Monthly averaged precipitation estimates for 1979-2010 from ERAi (red), ERAi detrended (black), and GPCP (blue), averaged for all ocean locations. Adapted from Dee et al. (2011).

Figure 11 shows the globally averaged annual precipitation in ERAi as a function of time. It exhibits large variations which act to modify strongly E-P through time (Figure 12). Three periods (or time intervals) of distinct behaviour can be identified.

- A period from 1979 to 1991 when precipitations are above the mean and exhibit no trend (Fig. 11). During that period, the globally averaged annual mean E-P in ERAi is close to 0.4 mm/day (Fig. 12).
- A period from 1992 to 2004 characterized by a large "jump" (or discontinuity) in 1992 when precipitation falls by 0.13 mm/day followed by a well marked negative trend (Fig. 11). The 1992 "jump" is also noticed in the E-P field (Fig. 12), and the negative trend in P contributes to the gradual rise of E-P up to values near 0.8 mm/day.
- A period from 2005 to 2012 characterized by a strong positive trend inducing the greatest change in precipitation seen in the whole time series (0.25 mm/day). E-P decreases by almost 0.2 mm/day during that period of time (Fig. 12).

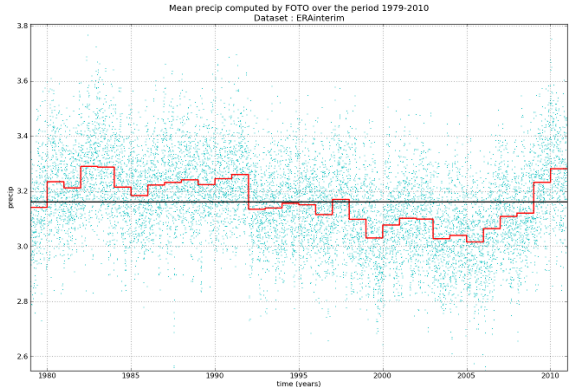

Figure 11. Globally averaged precipitation in the original ERAi (in mm/day). The blue dots are the daily values, and the red line shows the annual mean. The black line is the time mean over the whole period.

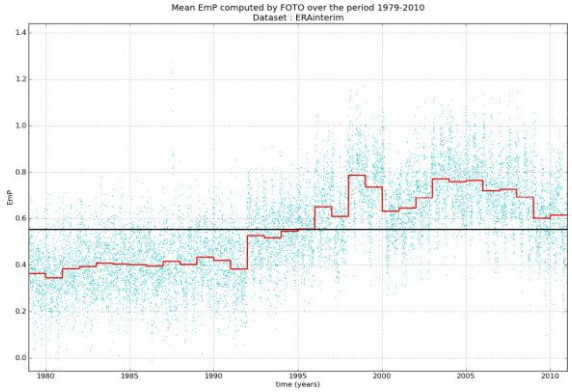

Figure 12. Globally averaged E-P in the original ERAi (in mm/day). The blue dots are the daily values, and the red line shows the annual mean. The black line is the time mean over the whole period.

Those discrepancies are likely to induce large-scale salinity drifts in ocean models. Given that uncertainties on precipitations are quite large, poor confidence should be given to those trends and discontinuities. Thus, it has been decided to correct the precipitations in order to stabilize the freshwater budget in time following an approach in two steps.

In the first step, we calculate and remove the linear trend of the precipitation time series for each of the 3 time intervals identified above independently (1979-1991; 1992-2004, 2005-2012). The process is applied at every grid point using the significant trend (two-tailed t-test) computed over the corresponding period. Figure 13 shows the result of that de-trending. Marked discontinuities (or "jumps") are clearly seen between the periods in 1992 and 2005, as the result of the piecewise de-trending approach.

In a second step, for each period, the de-trended precipitation fields have been rescaled to the original 1979-2010 mean of 3.16 mm/day to remove the "jumps" and to conserve the total precipitation over the full ERAi period. Figure 14 shows the result of the rescaling. The impact of

this correction on the E-P budget is a decrease by almost 0.2 mm/day, which goes in the right direction toward a closed E-P budget.

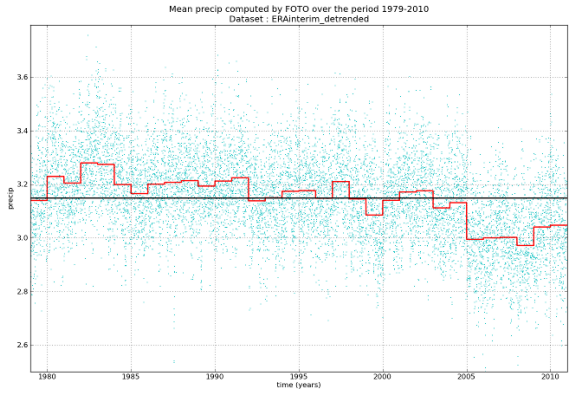

Figure 13. Globally averaged precipitation in ERAi after the application of the piecewise de-trending. The blue dots are the daily values, and the red line shows the annual mean. The black line is the time-mean over the whole period. Notice the steps in 1992 and 2005 due to de-trending by pieces and the mean value (black curve) is lower than in ERAi.

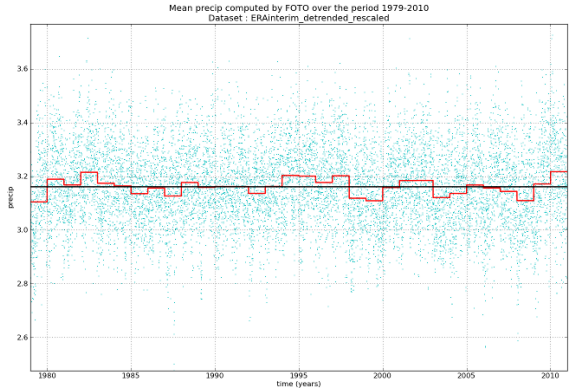

Figure 14. Globally averaged, de-trended and re-scaled precipitation in ERAi. The blue dots are the daily values, and the red line shows the annual mean. The black line is the time-mean over the whole period. There is no more discontinuity in 1992 and 2005.

Finally, we have applied the method of Storto (personal communication, 2013) to the de-trended precipitations with a few modifications. The method is designed to work online (in sbcblk_core module) in the case of an ORCA025 simulation. As our purpose is to provide a standalone corrected forcing set on the native ERAi grid, we adapted Storto's code to run it offline. However interpolation to ORCA025 was needed to apply the correction, thus fields have been interpolated twice: from native to ORCA025 grid before correction then from ORCA025 to native grid after correction.

Storto's method separates the large scales from the small scales precipitations with a dimensional low-pass Shapiro filter, tuned to have 20% amplitude attenuation at the spatial scales corresponding to 900km. A spatially varying, monthly climatological scaling coefficient is computed over the period 1989–2008 that accounts for the ratio between the ERAi large scale precipitation and a satellite-based passive microwave precipitation product (the PMWC product, Hilburn, 2009). The large scale ERAi precipitation is then scaled with this coefficient and the small scale precipitation are added back. Whereas Storto suggests to interpolating in time the correction term, we found it inappropriate because what we consider important to conserve the total amount of added (or retrieved) precipitations over the month.

Figure 15 shows the correction provided by Storto's method on original ERAi (not de-trended). Though the obtained corrected field (after de-trending) will be slightly different (see next section),

this illustrates the main effects of this correction. The correction decreases the mean precipitation in the western tropical Atlantic and Pacific oceans which will allow to reducing the freshwater biases found in ERAi-driven simulations in these regions. Precipitations are also increased in northern hemisphere subtropical gyres with a strong increase along Canadian east coast which is more surprising.

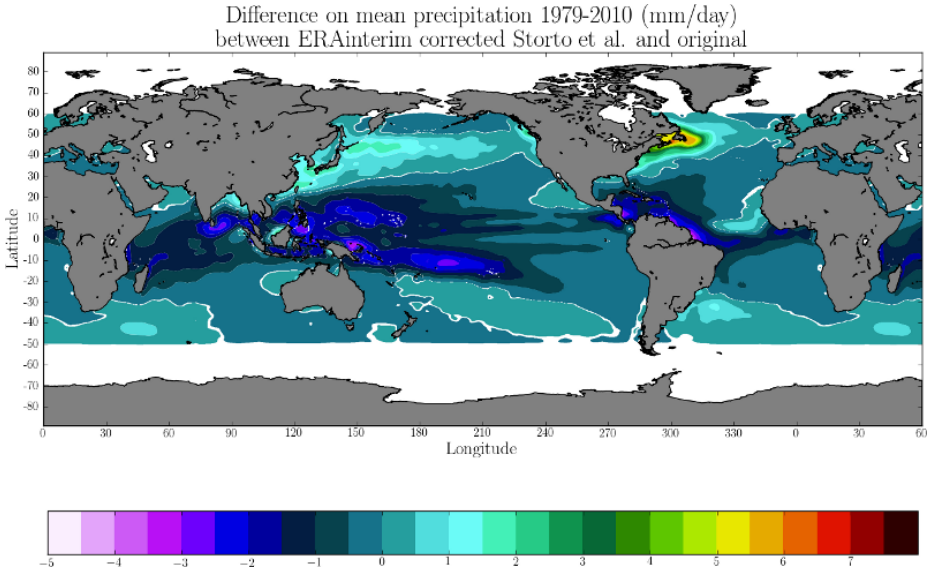

Figure 15. Mean (1979-2010) precipitation difference between the ERAi data corrected with Storto's method and original ERAi data.

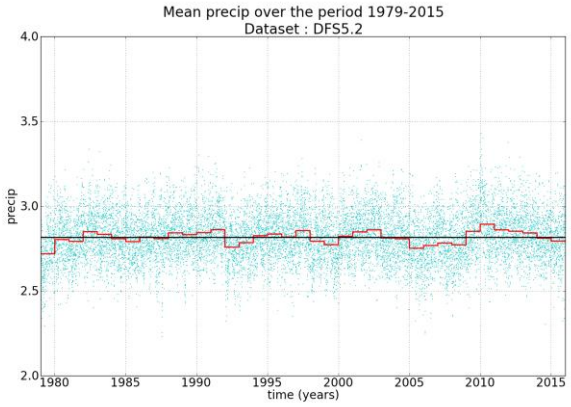

Figure 16. Globally averaged Precipitation in DFS5.2 with all corrections/de-trending applied. The blue dots are the daily values, and the red line shows the annual mean. The black line is the time-mean over the whole period.

In the next section, we show the results of all the modifications performed on ERAi. We focus on the differences between DFS5.2 and the original ERAi and provide information mostly on the climatological mean and interannual variations. This is presented as an atlas to give the essential information about DFS5.2. More exhaustive diagnostics are available in the FARC reports (available on demand: bernard.barnier@lgge.obs.ujf-grenoble.fr).

4 EXTENTION OF DFS5.2 TO THE PERIOD 1958-1978

This section describes the final stage of the making of DFS5.2: the extension of DFS5.2 backward in time over the years 1958 to 1978 using ERA40 reanalysis. The extension process yields the final DFS5.2 which covers the period 1958-2010 (recently extended to 2015). In the following, when fluxes are presented, they have been calculated using the Bulk formula of Large and Yeager (2004) and the inter-annually varying SST of Hurell et al. (2008).

4.1 Radiation and freshwater fluxes for 1958-1978

Regarding radiation (downward shortwave and longwave) and freshwater (total precipitation and snow) fluxes, the lack of observations before 1979 and the large flaws noticed in ERA40 reanalysis did not allow to produce reliable enough inter-annually varying fluxes. Therefore, we decided to use the daily climatology of DFS 5.2. This was also the strategy for DFS4 and is also the strategy used in CORE. The extension is illustrated in Fig. 17 with the shortwave radiation in the equatorial band and the global precipitation, respectively. There is a lack of high frequency variability for the period before 1979 due to the use of the daily climatology. However, the continuity of the record through 1979 is well assured and the whole record is centred on the 1979-2012 mean value.

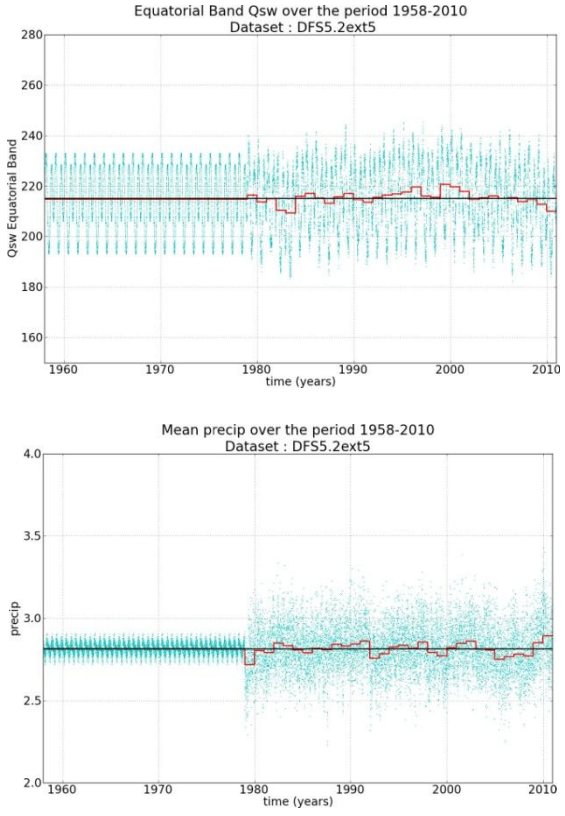

Figure 17. Time-series of (upper plot) the zonal average in the equatorial band of the shortwave radiation ($W.m^{-2}$) and (lower plot) the globally averaged precipitation in DFS5.2. Blue dots are daily values. The red line shows the annual mean. The black line is the time-mean over the whole period.

4.2 Turbulent fluxes for 1958-1978

For the atmospheric variables required for the calculation of the turbulent fluxes (t2, q2, u10 and v10), the strategy is much complex is based on an approach that combines DFS5.2 daily climatology to the high frequency of the synoptic scales of ERA40. This is done in several steps detailed below (Figure 18):

i. Compute the mean state for each variable: we produce a daily climatology for every variable of DFS5.2 for the period 1979-2010 and of ERA40 for the period 1958-1978.
ii. 6-hourly *residues* are computed for ERA40 over 1958-1978: we remove from the ERA40 full 6-hourly fields the ERA40 daily climatology computed above and remove any significant linear trend. ERA40 *residues* are interpolated to 3-hourly time frequency: to avoid changes in time frequency between the extended and standard periods, a linear interpolation is performed in time on the residues.
iii. The full fields for DFS5.2 over 1958-1978 is recomposed by adding the 3-hourly residues of ERA40 to the daily climatology of DFS5.2. All fields are given on the 0.7° original ERAi grid.

The resulting time-series are shown in Fig. 18 for the zonal wind component in different latitude bands. There is a rather good continuity between the two periods 1958-1978 and 1979-2010 and no major jumps in 1979. Though the effective time frequency over the period 1958-1978 is only 6 hours, the amplitude of the time-series is rather similar for the two periods.

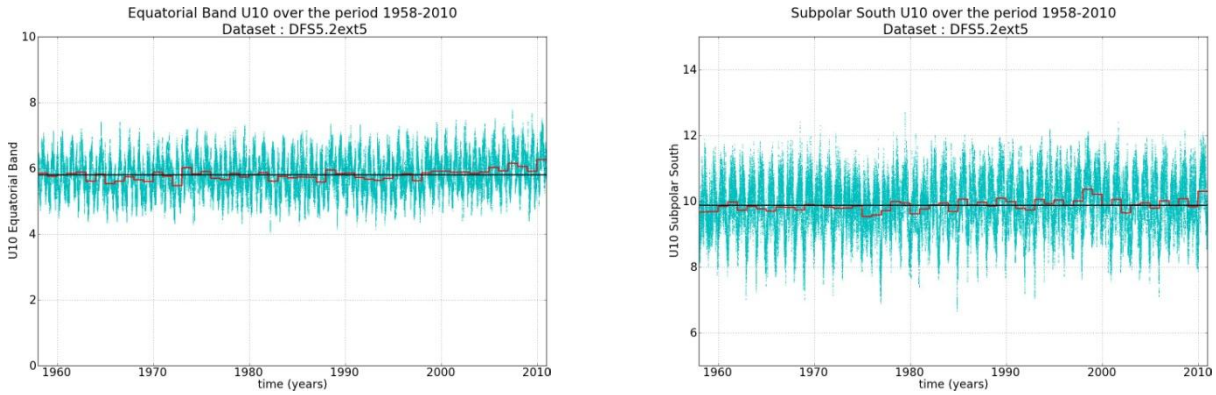

Figure 18: Zonal average of the zonal component of the 10 m wind in DFS5.2. Left: in the equatorial band (10°S-10°N). Right: in the Southern Ocean (45°S-70°S). The record shows a very continuity between the ERA40 and the ERAi periods. A small increasing trend is noticeable from the late 1990s to present in the equatorial band. A small increasing trend is noticeable from the mid 1970's to the late 1990's in the Southern Ocean. Blue dots are 3-hourly values. The red line shows the annual mean. The black line is the time-mean over the whole period.

Fig. 19a-c shows the global average of the net heat flux, Qnet, and of its two major components, the total radiation flux Qrad and the total turbulent flux Qtrb. There is no apparent "discontinuity" in 1979 when the ERA40 and ERAi data sets are joined. However, there is a clear shift between the two periods in term of mean value, shift mainly driven by Qtrb (and more specifically by the latent heat flux). Qtrb does not vary much over the first 20 years of the record (nearly 115 Wm^{-2} from 1958 to 1976), but increases rapidly by nearly 10 Wm^{-2} between 1977 and 1984 (without any marked discontinuity in 1979). Qtrb shows an increasing trend for the rest of the period (from the 1980's to present), trend also seen in COREv2. The global freshwater flux (not including runoff) E-P, shown in Fig 19d, exhibits a discontinuity in 1979, comparable to the change in P seen in 1998 or 1999. It is mainly driven by P and by the shift from daily climatology to inter-annually varying (see Fig. 17).

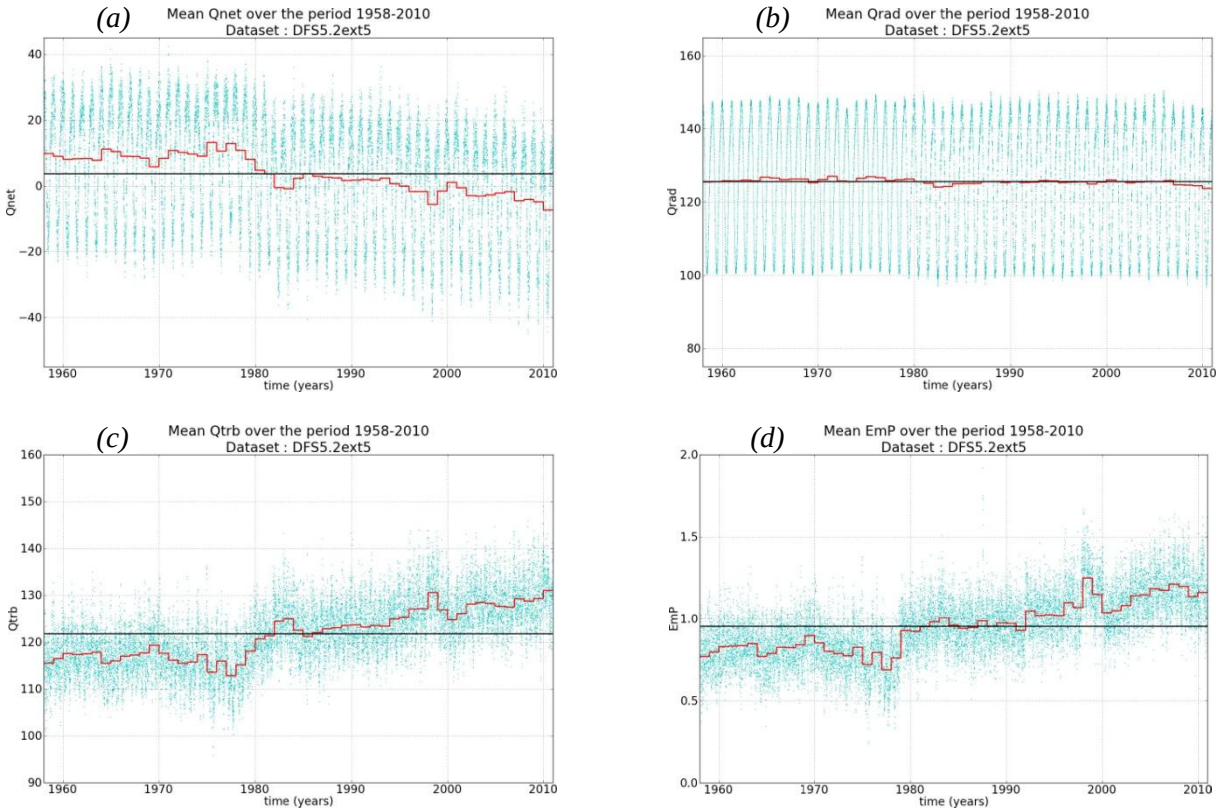

Figure 19. Global average of (a) the Net Heat Flux Qnet and its two major components, the total radiation flux Qrad (b) and the total turbulent flux Qtrb (c).Units are in Wm^{-2}. The global freshwater flux (not including runoff) E-P (mm/day) is shown in (d). Blue dots are 3-hourly values. The red line shows the annual mean. The black line is the time-mean over the whole period.

4.3 Comment of continuity in 1979

The above analysis of the various flux components of DFS5.2 does not show any significant discontinuity in 1979 when ERA40 and ERAi are joined, except on the E-P field which shows a shift of ~ +0.2mm/day.

However, the global latent heat flux shows a significant but regular increase between 1976 and 1984 which imprints on the net heat flux (Fig. 19). In total this increase is ~10 Wm^{-2} over this almost 10-year long period. This signal is mainly due to ERAi which shows an increase in *Qtr* of about 7 Wm^{-2} spanning years 1979 to 1984 (black circle in Fig. 20).

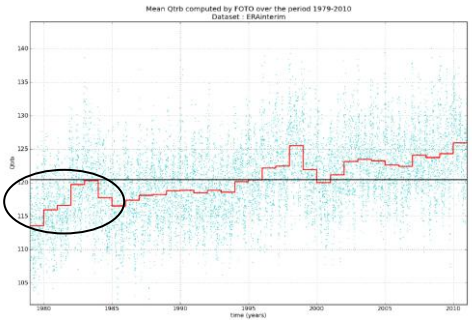

Figure 20: Global average of the total turbulent flux Qtrb in the original ERAi. Units are in Wm^{-2}.

5 COMPARING DFS5.2 AND ERAi ORIGINAL FIELDS

This section presents the differences between the 1979-2015 climatologies of DFS5.2 and original ERAi, to illustrating the impact of the corrections on the mean.

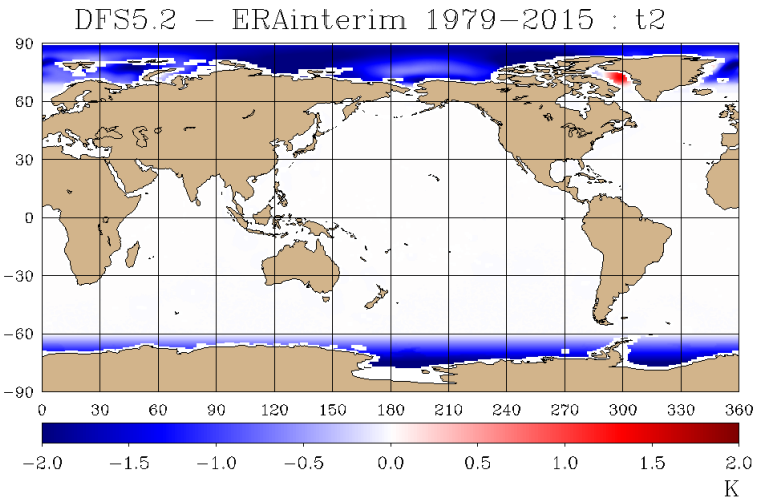

Fig. 21: Difference DFS5.2 minus ERAi (1979-2015 annual mean): Air Temperature at 2 m.

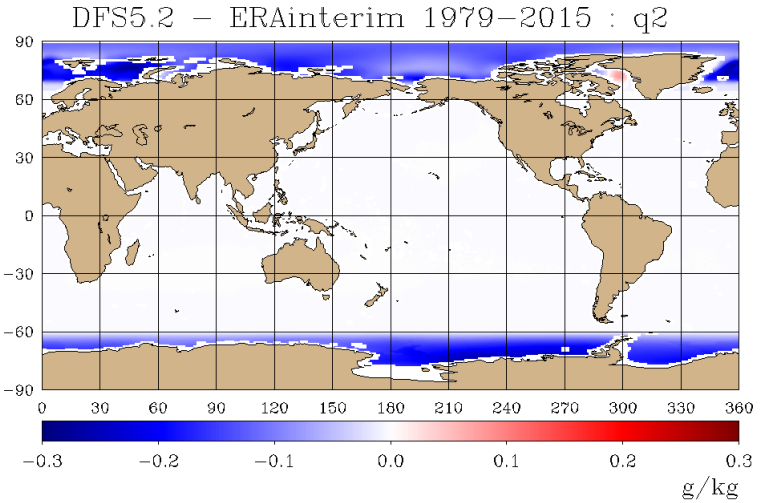

Fig. 22: Difference DFS5.2 minus ERAi (1979-2015 annual mean): Air Specific Humidity at 2 m.

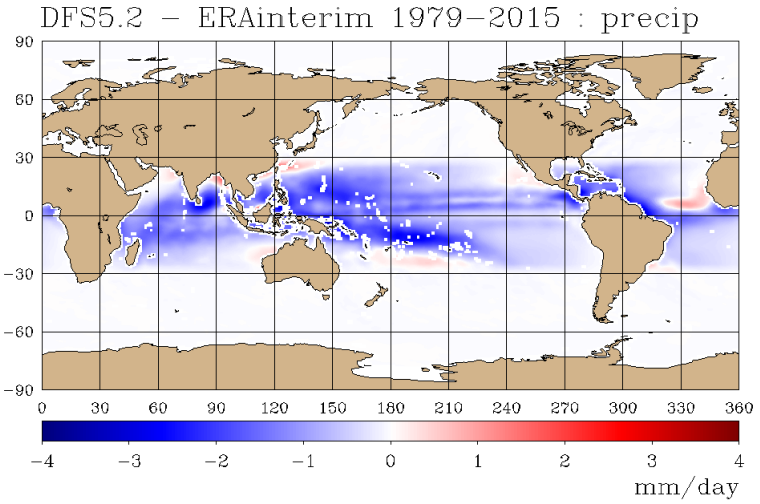

Fig. 23: Difference DFS5.2 minus ERAi (1979-2015 annual mean): Liquid Precipitation.

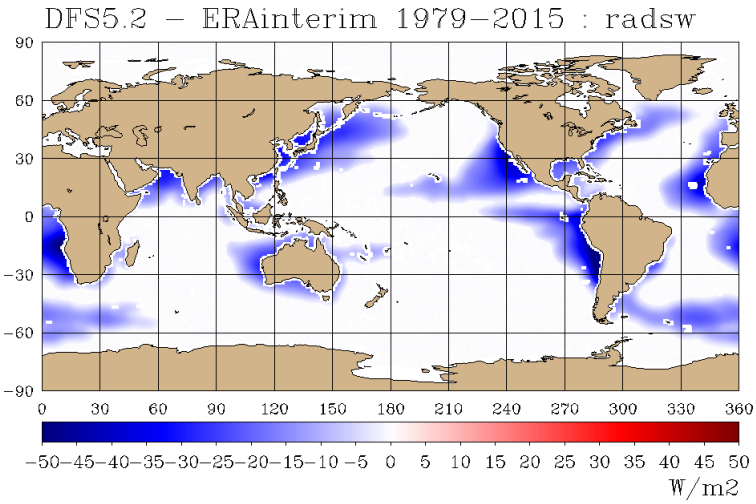

Fig. 24: Difference DFS5.2 minus ERAi (1979-2015 annual mean): Downward Shortwave Radiation.

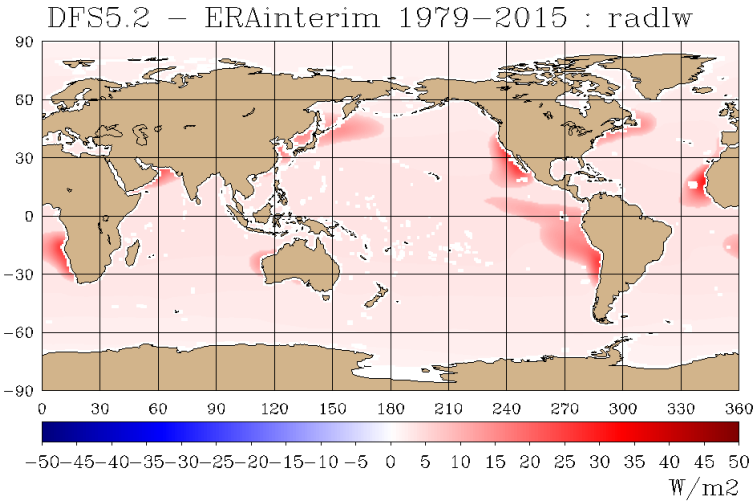

Fig. 25: Difference DFS5.2 minus ERAi (1979-2015 annual mean): Downward Longwave Radiation.

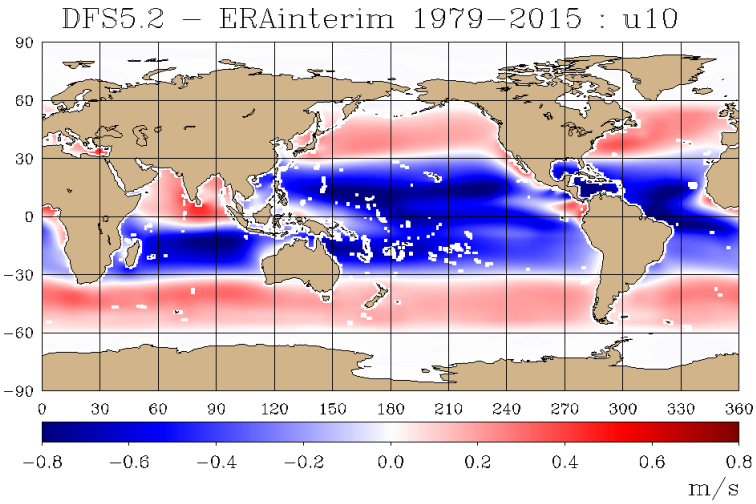

Fig. 26: Difference DFS5.2 minus ERAi (1979-2015 annual mean): Zonal Wind Speed.

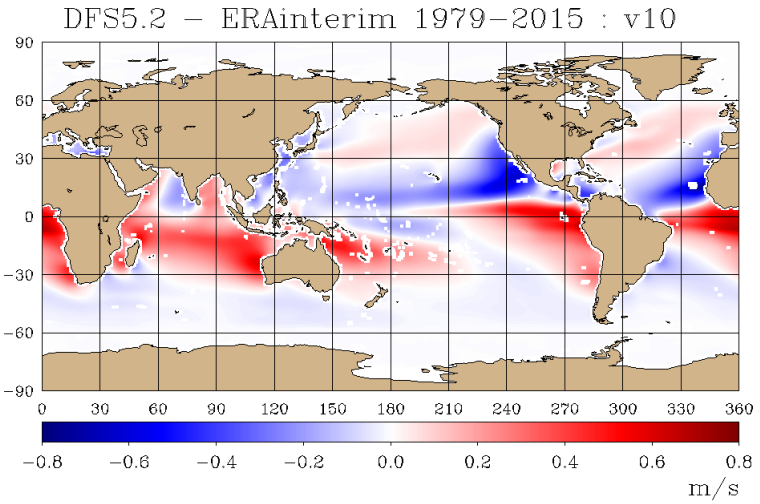

Fig. 27: Difference DFS5.2 minus ERAi (1979-2015 annual mean): Meridional Wind Speed.

5.1 Impact of TOA mooring in DFS forcing

Josey et al. (2014) identified a pattern of strong near surface humidity anomalies, co-located with the TAOmooring array array in the original ERAi which significantly imprint on DFS5.2 (Fig. 28). The pattern generates large, previously unrecognized latent and net air-sea heat flux anomalies, up to 50W.m^{-2}.

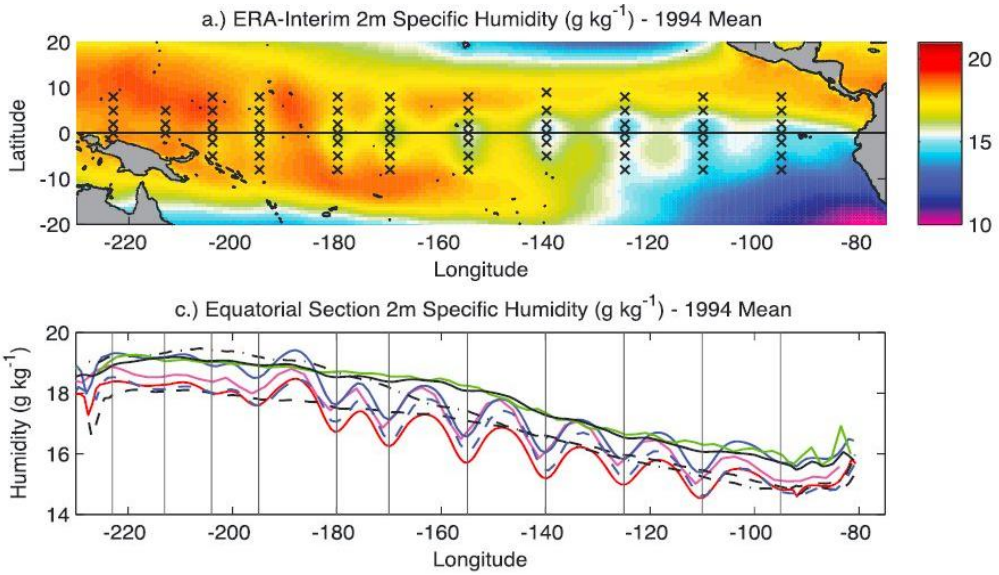

Fig. 28: (Top) 1994 annual mean of ERA-Interim 2m specific humidity. Mooring locations are indicated by the black crosses. (Bottom) Equatorial section of 1994 mean specific humidity for Drakkar Forcing Set (DFS) (dashed blue), ERA-Interim (red), ERA40 (magenta), MERRA (black dash-dot), NCEP/NCAR (green), CFSR) (black dashed), OAFlux (black), and TropFlux (blue). After Josey et al., (2014).

6 ISSUES WITH DFS5.2 REVEALED BY ORCA SIMULATIONS

Simulations driven by DFS5.2 have been carried out at LGGE with the Drakkar hierarchy of ORCA simulations at 1/2°, 1/4° and 1/12°. Several issues noticed with this forcing are reported below. Figures presented below show the results for the period 1958-2012, but simulations have been continued to 2015.

6.1 Global Drifts

T, S and SSH global drifts are compared between DFS4.4 and DFS5.2 in 1/2°, 1/4° and 1/12° simulations (Fig. 29, 30). We mention here that drifts are generally not robust (in sign or amplitude) to changes in grid resolutions. Or interpretation of this is that global drifts results from an imbalance between regional biases, and that these regional biases are sensitive to resolution.

DFS5.2 forcing produces significantly smaller drifts in S and SSH than DFS4.4 and this holds for both resolutions. In particular, these drifts are almost zero in ORCA025 (Fig. 30). Note that the S and SSH drifts change signs between 1/4° and 1/12°. The small amplitude of those drifts only indicates a better compensation and not a reduction of the regional biases.

The T drift is very consistent between DFS5.2 and DFS4.4, both showing a cooling of the global ocean, greater in DFS4.4 at the resolution of 1/12° (~ -0.05°C over the whole period), and inversely, greater in DFS5.2 at the resolution of 1/4° (~ -0.015°C). Note that the ORCA05 (1/2°) simulation shows a warming (~ +0.03°C, no figure shown).

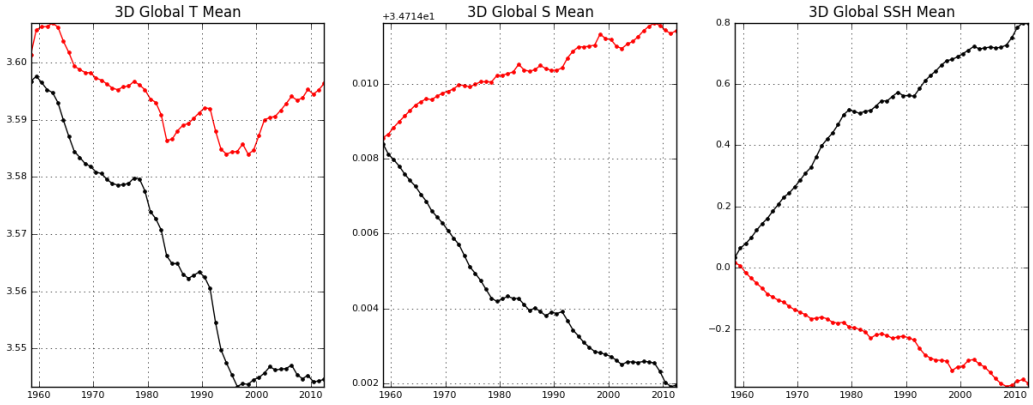

*Figure 29: Global Temperature (T), Salinity (S) and Sea Surface Height (SSH) in ORCA12 (1/12°) runs driven by **DFS4.4 (black)** and **DFS5.2 (red)**.*

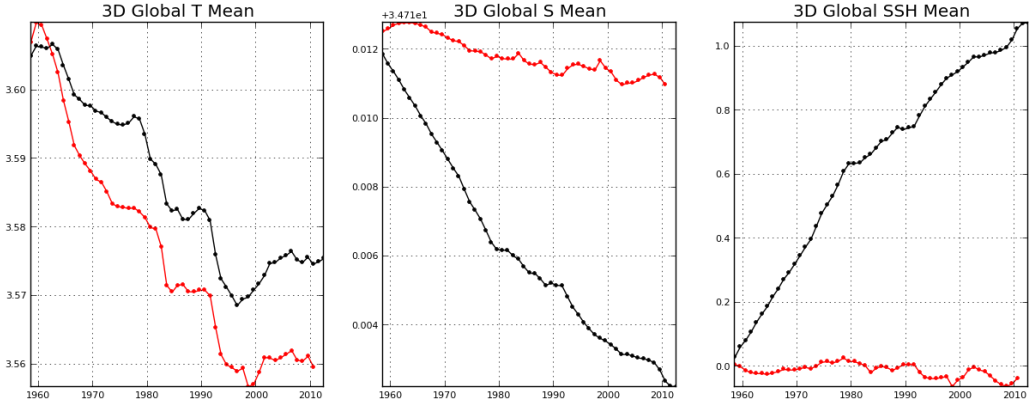

*Figure 30: Global Temperature (T), Salinity (S) and Sea Surface Height (SSH) in ORCA025 (1/4°) runs driven by **DFS4.4 (black)** and **DFS5.2 (red)**.*

6.2 Atlantic Meridional Overturning

The AMOC produced by DFS5.2 and DFS4.4 (Fig. 31) are very comparable in ORCA12 in terms of mean value, trends and variability. The same holds in ORCA025 except for the mean which is is greater by 1 Sv with DFS5.2.

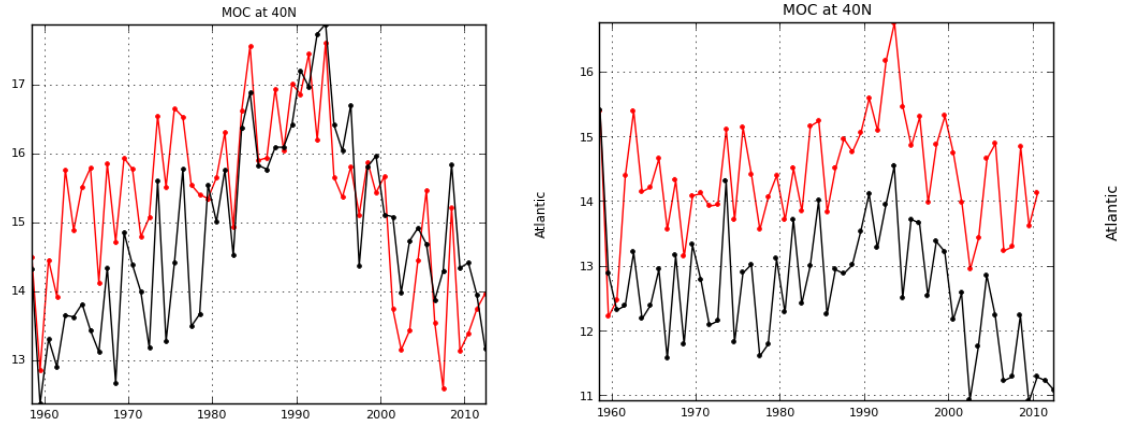

(a) ORCA12 (b) ORCA025

*Figure 31: Evolution of the AMOC at 40°N in (a) ORCA12 (1/12°) and (b) ORCA025 (1/4°) runs driven by **DFS4.4 (black)** and **DFS5.2 (red)**.*

6.3 Florida Strait Transport

The volume transport at the Florida Strait(Fig. 32) is very comparable between the DFS5.2 and DFS4.4 simulations in the 1/12° simulation. In the ORCA025 simulations, this transport is systematically greater in DFS5.2 from the 1940s to the end of the run. We notice a collapse of this transport in all DFS4.4 simulations starting in 1998.

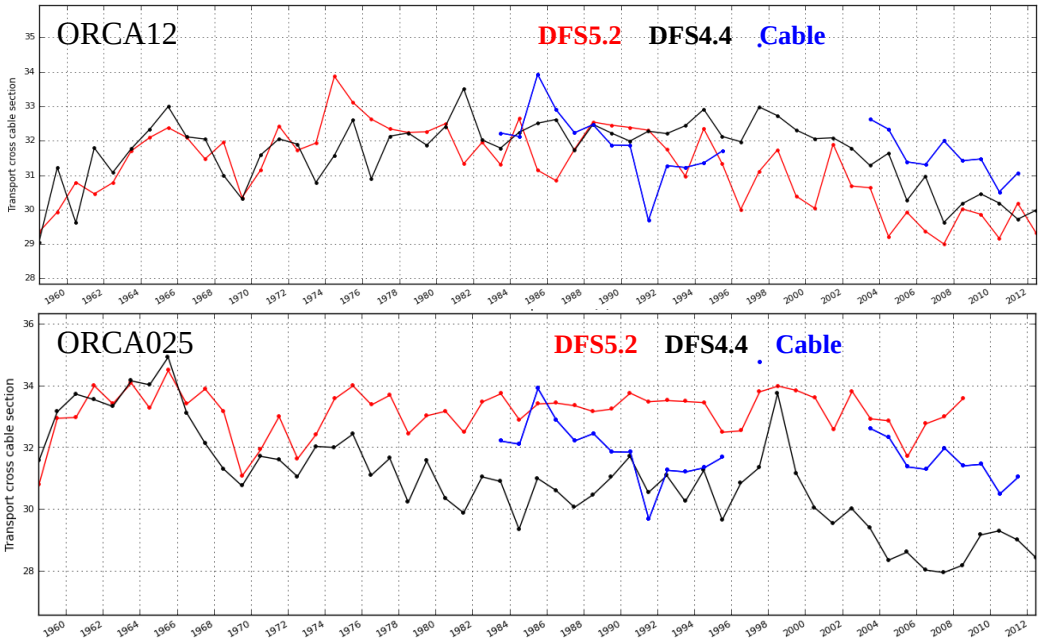

Figure 32. Annual mean time-series of the volume transport (in Sv) at the Florida Strait and its comparison with the Cable measurements.

6.4 Weddell Sea Polynya

The opening of Polynyas in the Weddell Sea is a recurrent issue in Drakkar simulations. The ORCA025 simulation shows an opening of a polynya in the early 1980s (Fig. 33) that persists until the end of the run in 2015. It is worth to mention that the ORCA025 simulation driven by DFS4.4 did not show any Polynya opening (no figure shown).

The ORCA12 simulation driven with DFS5.2 also showed a Polynya opening in the early 1980s. (The run was re-started frm 1979 with a local T,S relaxation in the surface that allowed to prevent the Polynya to appear).

Note that the simulation ORCA05 (1/2°) driven with DFS5.2 did not show any Polynya opening during the whole run (no figure shown).

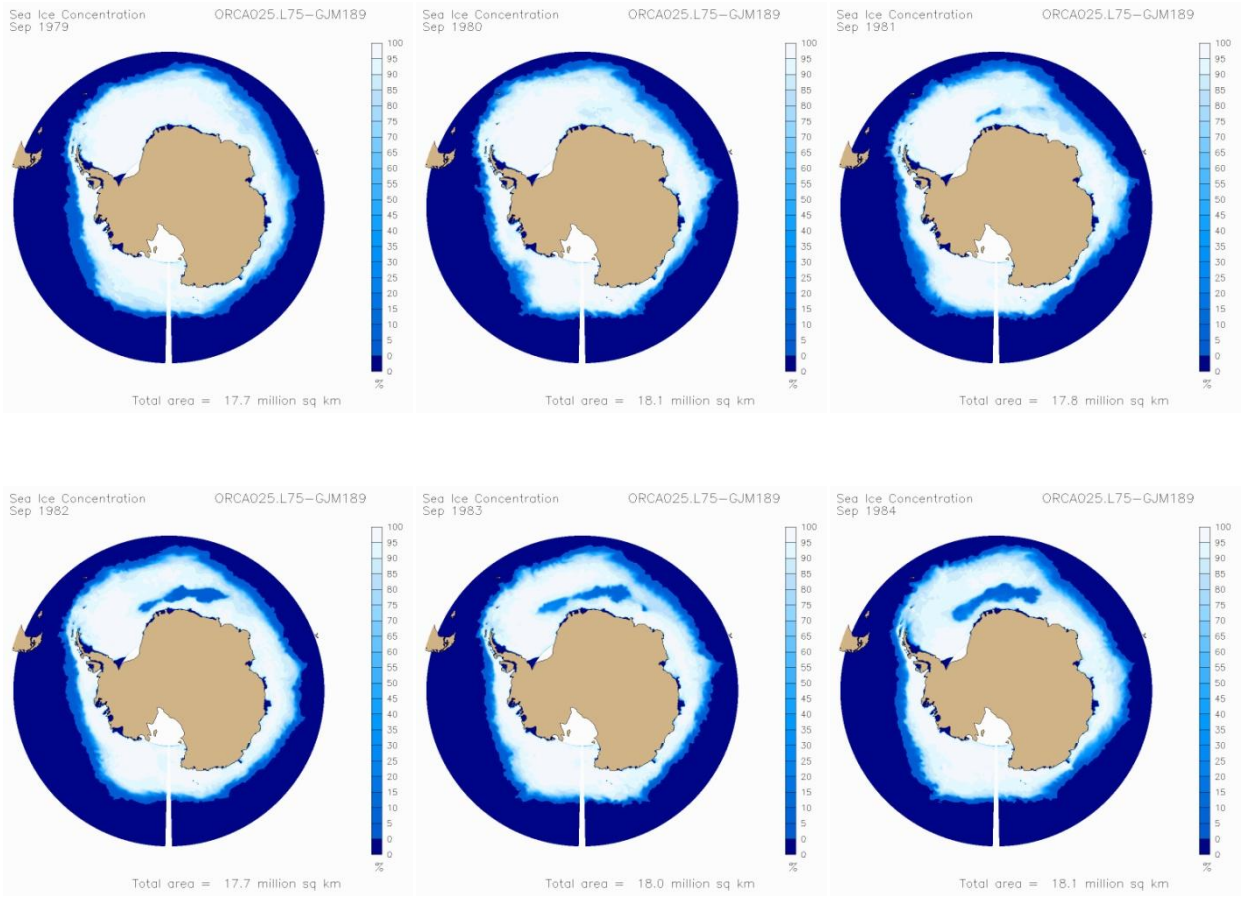

Figure 33: September-mean Sea Ice concentration in an ORCA025 simulation driven by DFS5.2 from 1979 to 1983 (ORCA025.L75-GJM189).The beginnings of the Weddell Sea polynya are visible in 1980. The Polynya area is then growing.

6.5 Arctic Sea Ice

The total volume of sea-ice in the Arctic (Fig. 34) is greater in DFS4.4 from the beginning of the run until the early 1990s. Both forcing represents the collapse of sea-ice in summer from the mid 1990s, and in particular the minimum of 2007, but both overestimate the sea-ice area and extent in summer, DFS4.4 being however closer to observations than DFS5.2. ORCA12 clearly represents an improvement compared to ORCA025.

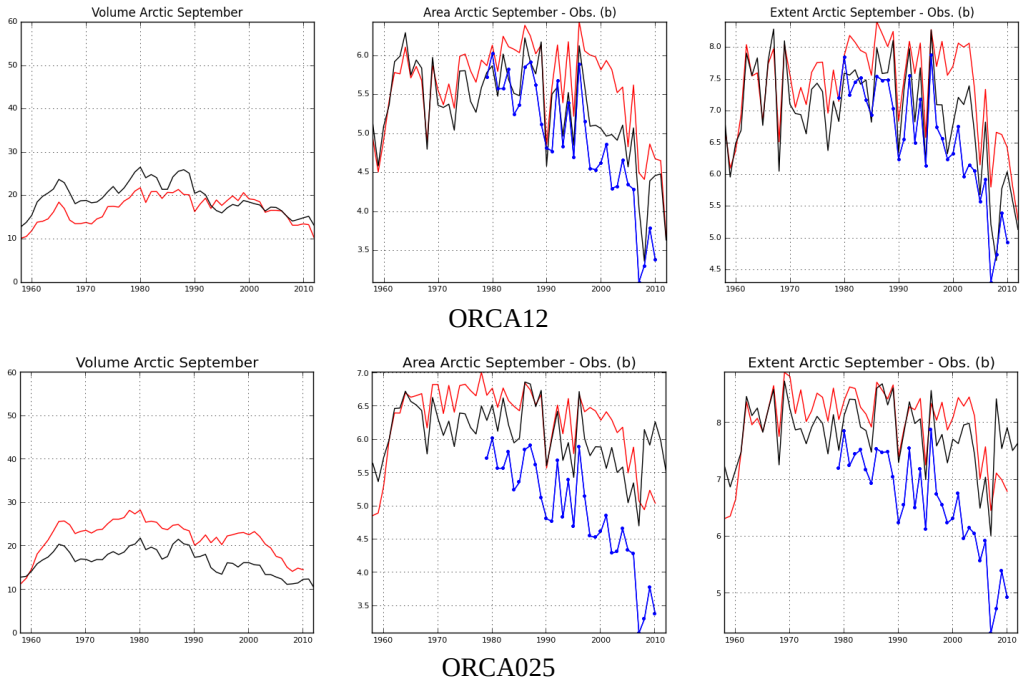

*Figure 34: Time series of volume, Area and Extent of the sea-ice in the Arctic ocean in (top) ORCA12 and (bottom) ORCA025 simulations. In **blue** the **satellite estimates**, in **black DFS4.4** and in **red DFS5.2**.*

6.6 North Atlantic dense water overflow

The flow of dense water (σ_0 > 27.8) at the sills of the Denmark Strait and the Faroes Bank Channel (Fig. 35) is rather constant in ORCA12, indicating a continuous production of dense water in the GIN Seas. DFS4.4 produces a greater transport at Denmark Strait than DFS5.2, but both show similar variability. In ORCA025 runs, both forcing produce a overflow of dense waters that diminishes with time (no Fig. shown).

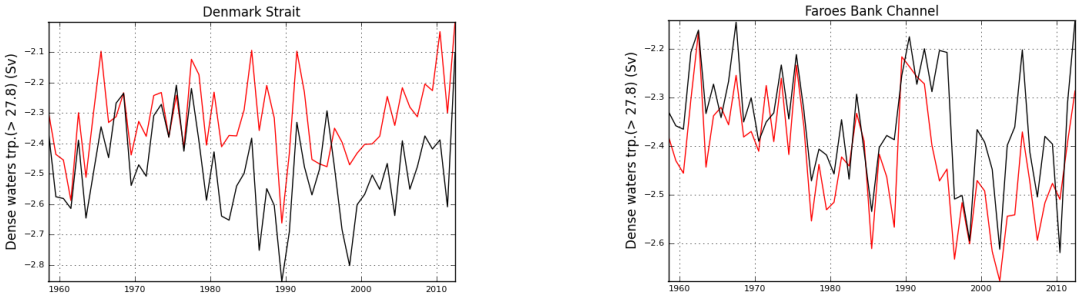

*Figure 35: Transport time series (in Sv) of water denser than σ_0 = 27.8 at the Denmark Strait (top) and at the Faroe Bank Channel (bottom). In **red** the transport for **DFS5.2** and in **black** the transport of **DFS4.4**.*

7 BRIEF ASSESSMENT OF THE ORIGINAL ERAi

ERAi is a recent reanalysis provided by ECMWF (Dee et al., 2011). It covers the period 1979-2013. Many improvements have been implemented to both the atmospheric model and the data assimilation system compared to ERA-40, which was the basis for DRAKKAR Forcing Set 4.3 and 4.4. The spatial and temporal resolutions have also been increased (0.7° and 3-hourly for ERAi, 1.125° and 6-hourly for ERA-40). Despite a better representation of the atmospheric state, the reanalysis still has some flaws which may significantly impact the solution of an ocean model. In order to guide the search for corrections to be applied to ERAi, we carried-out a global ocean hindcasts simulation with the global 1/4° global ORCA025.L75 configuration. This simulation is referred to ORCA025.L75.MJM95.

7.1 Gyre intensity

Figure 36 shows the transport across the Florida-Bahamas section, which is a good proxy for North-Atlantic subtropical gyre intensity. This section is monitored and observations (in blue) are available since 1982. We compare a DFS4.3 forced ORCA025 simulation (in black) and an ERA-interim forced ORCA025.L75 simulation (in red). The transport collapses in the ERA-interim forced simulation, which is the result of a weakening of the subtropical gyre circulation. This behaviour is observed in a large number of ERA-interim forced simulations performed by the DRAKKAR group and is not due to vertical resolution, nor to spin-up. Hence we can conclude that gyre circulation has to be strengthened, which can be achieved by increasing the wind module. The weak winds in ERAi has also been pointed out in the study of Meinvielle et al. (2013) which suggests an underestimation of the wind speed by 0.5 m/s in the inter-tropical band.

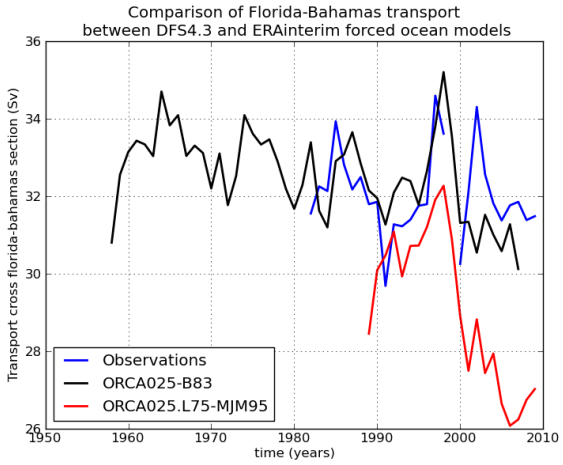

*Figure 36. The Florida-Bahamas transport in two different ORCA025 hincast simulations is shown. One is driven by DFS4.3 forcing (**black**) and the other is driven by ERAi raw forcing (**red**). The Cable observations are in **blue**.*

7.2 Freshwater input

Figure 37 shows the sea surface salinity restoring term in an ERAi forced ORCA025.L75 simulation. We can identify several areas where the restoring term is important: the western equatorial Pacific and Indian oceans, the equatorial Atlantic and along US/Canada East coast. The precipitations are intense and likely overestimated at low latitudes and underestimated at mid-latitudes. Similar results were found comparing ERAi to other precipitation estimates satellite or other reanalyses (Sommer, 2013). ERAi provides daily precipitations at 0.7° resolution, which brings more variability to the system than the monthly satellite-based precipitations of DFS4.3. However, to be useful, the precipitations need to be in good agreement with observations. Hence a major issue is to decrease precipitations at low-latitude which will affect the global hydrological cycle, which is already not balanced in ERAi, showing an excess of evaporation (E-P-R = 0.33 mm/day). Despite of this non-balanced freshwater budget, simulations forced by ERAi without sea

surface salinity restoring show an important negative salinity drift (freshening), leading to a sea surface rise of 50-60 cm in 20 years in both ORCA2 and ORCA025 simulations.

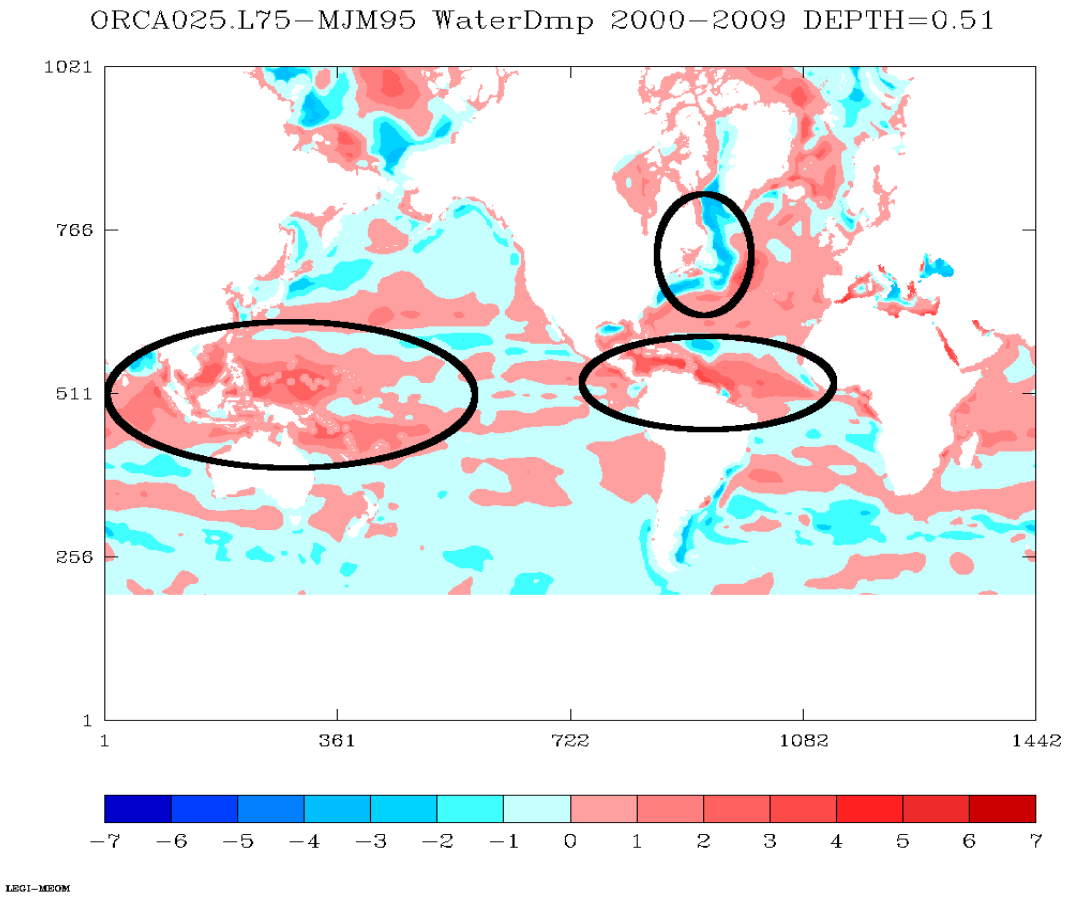

Figure 37: Mean Sea Surface Salinity restoring term in an ERAi forced simulation (2000-2009 mean). Positive (red) values means that the restoring acts similarly as evaporation, negative (blue) values means that the restoring brings freshwater.

7.3 Radiation fluxes

ERAi also provides daily radiation fluxes at 0.7° resolution, whereas satellite-based DFS4.3 radiation fluxes have only a 2.5° resolution. Figures 38&39 show the difference in downward shortwave and longwave radiation between ERAi and DFS4.3 (the latter being basically the satellite ISCCP product). ERAi shortwave radiations are likely overestimated (the difference with DFS4.3 being positive almost everywhere), in particular in the eastern part of ocean basins. In these latter regions the difference in longwave radiation is negative (ERAi providing less downward longwave radiation), which suggests that the discrepancies in the radiation fluxes between ERAi and satellite products are due to flaws in cloud cover representation.

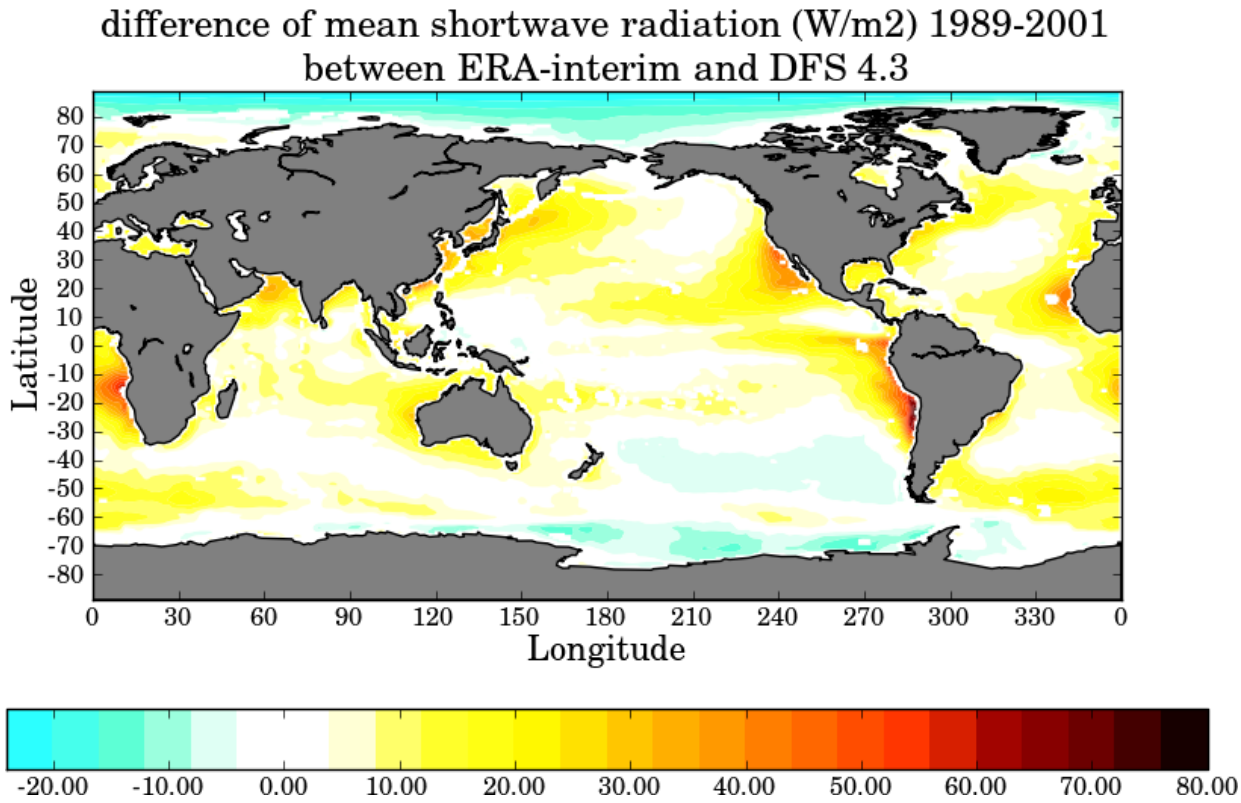

Figure 38. Difference between ERAi and DFS4.3 downward shortwave radiation (mean 1989-2001)

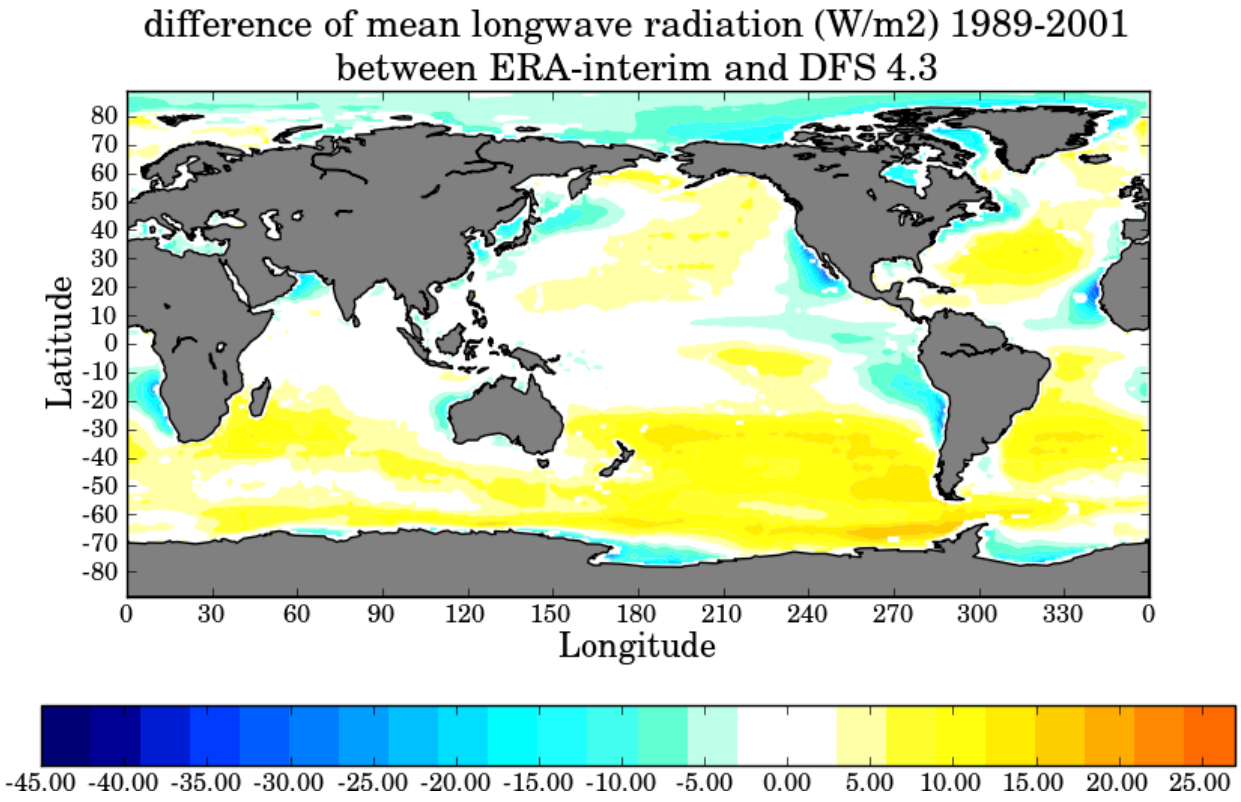

Figure 39. Difference between ERAi and DFS4.3 downward longwave radiation (mean 1989-2001).

8 BRIEF DESCRIPTION OF THE PREVIOUS DFS

This section briefly recalls the main characteristics of the previous Drakkar Forcing Sets that have been used to drive ocean hindcasts of the period 1958 to present (see also Table 1). Every DFS forcing comprises the following surface variables required by the NEMO bulk formula to calculate heat, freshwater and momentum fluxes across the air-sea interface (i.e. the surface boundary condition to the model primitive equations).

- zonal and meridional components of the 10-m wind : *u10, v10*
- 2-m air humidity : *q2*
- 2-m air temperature : *t2*
- downward shortwave radiation at the sea surface : *radsw*
- downward longwave radiation at the sea surface : *radlw*
- precipitation total and solid : *P, snow*

8.1 DFS3 (period 1958-2007)

DFS3 covers the period 1958-2007. The reference for this forcing data set is the DFS3 data set described in the paper by Brodeau et al. (2010). The ORCA025 reference experiment driven with DFS3 is ORCA025.G70. DFS3 combines elements from two sources. The CORE_v1 forcing data set (Large and Yeager, 2004), from which precipitation (rain *P*, and *snow*), downward shortwave (*radsw*) and longwave (*radlw*) radiations are extracted. The ERA40 reanalysis (for the period 1958-2001) and ECMWF operational analysis (2002-2007) provide the 10-m wind (*u10, v10*), the 2-m air humidity (*q2*) and 2-m air temperature (*t2*) to compute turbulent air/sea and air/sea-ice fluxes during model integration. The frequency of DFS3 is monthly for precipitation and daily for radiation (both on the NCEP 1.875° grid), and 6-hourly for turbulent variables (on the 1.125° ERA40 grid). Note that climatological values are used for downward radiation and precipitation before 1979 as in CORE_v1 (see Table 1). The global heat and freshwater budgets (+12.8 Wm^{-2} and +56 mm/y, respectively) are not closed in DFS3.

8.2 DFS4.1 (1958-2007)

DFS4.1 is a significant evolution of DFS3. Corrections have been applied to ECMWF variables (used in the calculation of the turbulent fluxes) to remove unrealistic time discontinuities induced by changes in the nature of assimilated observations and by continuing ERA40 with ECMWF operational analyses, and to correct for obvious global and regional biases in ERA40 identified by comparison to high quality observations (see Brodeau et al., 2010). Winds have been rescaled such that the climatological mean matches that of the QuickScat winds. Air temperature and humidity have been corrected (i.e. cooled and dried) in the Arctic according to the POLES climatology (Rigor et al., 2000). Radiation fields are from ISCCP-FD (Zhang et al., 2004) with the reduction of 5% as proposed in CORE_v1. Precipitation is from the GXGXS data set (Large and Yeager, 2004). Both radiation and Precipitation have been submitted to small adjustments (in zonal mean) that yield a near-zero global imbalance of heat and freshwater when fluxes are estimated with the observed SST of Hurrell et al. (2008). The frequency and grid of DFS4.1 are as in DFS3 (Table 1).

8.3 DSF4.2 (1958-2007)

DFS4.2 is a small evolution of DFS4.1. The scaling coefficient applied to the 10m wind is slightly reduced by limiting the amplitude of the correction to a maximum of 15% (considering that QuickScat may overestimate the surface wind speed). A very small correction of t2 and q2 (corresponding to an offset of 0.25°C) is added in the latitude band 55°N-65°N for a better continuity with POLES in the Arctic.

8.4 DFS4.3 (1958-2007, extended to 2010)

For the period 1958-2007, DFS4.3 is exactly the DFS4 described in the Brodeau et al (2010) paper. It basically uses the corrections made and tested in DFS4.1 and DFS4.2, and adds new ones in order to close the heat and freshwater budgets.

Corrections applied to the 10 m wind and to the 2m air temperature and humidity to remove the unrealistic time discontinuities are retained as defined in DFS4.1 and DFS4.2. We recall that these discontinuities are induced by the changes in the nature of assimilated observations and by the use of ECMWF operational forecasts after 2001.

Corrections applied to 2m air temperature t2 and humidity q2 (i.e. cooled and dried) in the Arctic according to the POLES climatology are retained as defined in DFS4.1 and DFS4.2. *A small correction (equivalent to a 0.25°C offset) is added in the latitude band 55°N-65°N for a smoother connection with POLES*.

Rescaling of the 10m wind speed according to QuickScat in the band 60°S-60°N is retained as defined in DFS4.1 and DFS4.2. *However, the maximum amplitude of the rescaling is bounded to a maximum of 15%*.

Radiation fields from ISCCP-FD (Zhang et al., 2004) are reduced by 7 % in the inter-tropics, in a way similar that what was proposed by Large and Yeager (2004) for CORE_v1 (with a lesser reduction of 5%).

Precipitation from the GXGXS data set (Large and Yeager, 2004) are increased by 10% between 20°S-20°N to reach the values proposed by Trocolli and Kallberg (2004), and by 5% elsewhere.

Those adjustments yield a near-zero global imbalance of heat budget (+0.3 Wm^{-2}) and freshwater budget (-0.2 mm/y) when fluxes are estimated with the observed SST of Hurrell et al. (2008). The extension for 2008 to 2010 uses ERAi for the surface variables used in the calculation of the turbulent fluxes (u10, v10, t2, q2), and applies the persistence of year 2007 for the radiation fluxes and precipitation.

8.5 DFS4.4 (1958-2012)

DFS4.4 is the last forcing set of the DFS4 series (see Table 1 for a summary of characteristics). It is identical to DFS4.3 until 2001. The major evolution concerns the period from 2002 to 2012. For that period DFS4.4 uses ERAi for *every forcing variable* (i.e. the surface atmospheric variables used in the calculation of the turbulent fluxes, but also the downward longwave and shortwave radiation and rain/snow precipitation) in the following way.

- First the 3-hourly, ~0.7°x0.7° ERAi is interpolated in space onto DFS4.3 grids (i.e. onto the ERA40 grid for t2/q2/u10/v10, onto the CORE grid for radsw/radlw/P/Snow) and degraded to the DFS4.3 frequencies (to 6 hourly snapshots for the turbulent state variables, to daily mean for the downward radiation fluxes, and to monthly mean for the precipitation/snow).

- Then, "*high frequency residues*" are calculated as the difference between instantaneous original ERAi fields and the ERAi daily (monthly for precipitation) mean climatology (calculated over the period 1979-2001 common to ERA40 and ERAi). These "*residues*" are 6 hourly for the turbulent variables, daily for radiation and monthly for precipitation.

- Finally, the DFS4.4 field for the period 2002-2012 is calculated by adding the daily (monthly for precipitation) climatology of DFS4.3 to the ERAi *residues*. Here the DFS4.3 climatology is calculated over the common period 1979-2001.

This processing has the effect to remove the offset of ERAi with regard to DFS4.3 whereas preserving the full ERAi variability, and to produce a resolution (time and grid) which is identical to that of DFS4.3 (see Table 1).

8.6 DFS4.4_clim

A seasonal climatological forcing has been calculated from DFS4.4, which required a specific processing to account for the non linearity of the bulk formula. First the daily mean climatology is calculated for variables t2, q2 radsw, radlw by a simple time averaging of the 6-hourly or daily values over the whole 1958-2012 period. A 2-passes Hanning filter is then applied to produce 360 climatological days.

For the wind, using the daily climatology of u10 and v10 in the bulk formula will result in an underestimation of the momentum and heat input of at least 20 to 30%. Bulk formulas are such that it is the wind speed $w10 = (u10^2+v10^2)^{1/2}$ and the components of the pseudo stress *w10.u10*, *w10.v10* that are used. We therefore calculated the daily climatology of these terms and also applied a 2-passes Hanning filter. DFS4.4clim has consequently one additional variable, *w10*, and the zonal and meridional components of the wind are replaced by the zonal and meridional components of the pseudo-stress. Note that *w10* is used in the calculation of the exchange coefficients. The non-linear effect induced in the high frequency variations of the wind on the fluxes is therefore better represented.

DFS4.4_clim has been used for long climatological runs (e.g. the ORCA12.L46.GJM02 run for 85 years). Differences in net heat flux between the two data sets over the whole period generally range between ±5 W.m^{-2}, with however greater differences (up to 20 W.m^{-2}) seen in western boundary currents (Figure 40).

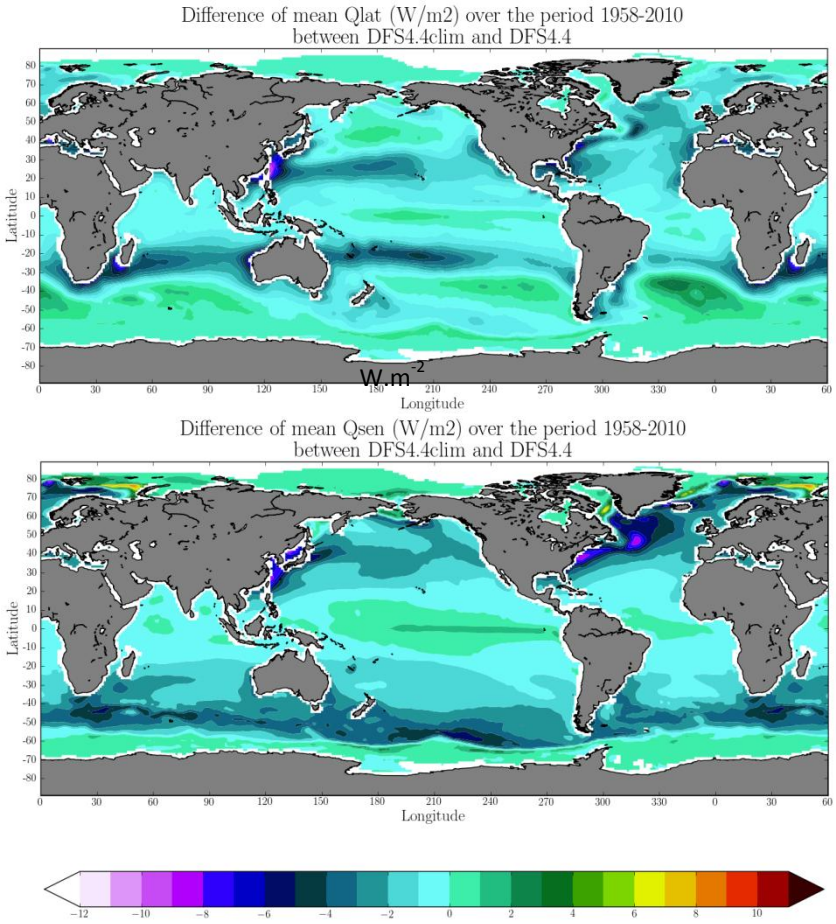

Figure 40: Differences in Latent and Sensible heat flux between DFS4.4-clim and DFS4.4 for the period 1958-2010.

Table 1: Major characteristics of the DFS3 and DFS4 data sets.

<table>
<tr><th rowspan="2">Variable name</th><th rowspan="2">Description</th><th rowspan="2">Units</th><th colspan="3">DFS3 Origin, time and grid resolution</th><th colspan="3">DFS4.3 Origin, time and grid resolution</th><th colspan="3">DFS4.4 Origin, time and grid resolution</th></tr>
<tr><th>1958-1978</th><th>1979-2001</th><th>2002-2007</th><th>1958-1978</th><th>1978-2001</th><th>2002-2010</th><th>1958-1978</th><th>1979-2001</th><th>2002-2012</th></tr>
<tr><td>u10</td><td>Zonal wind speed at 10 m height</td><td>$m.s^{-1}$</td><td colspan="2" rowspan="4">ERA40
6h
1.125°</td><td rowspan="4">ECMWF operational analyses
6h
1.125°</td><td colspan="2" rowspan="4">ERA40*
6h
1.125°</td><td rowspan="4">ECMWF operational analyses until 2007 and ERAi after
6h
1.125°</td><td colspan="2" rowspan="4">ERA40*
6h
1.125°</td><td rowspan="4">ERAi**
6h
1.125°</td></tr>
<tr><td>v10</td><td>Meridional wind speed at 10 m height</td><td>$m.s^{-1}$</td></tr>
<tr><td>t2</td><td>Air temperature at 2 m height</td><td>°C</td></tr>
<tr><td>q2</td><td>Air specific humidity at 2 m height</td><td>kg/kg</td></tr>
<tr><td>radsw</td><td>Downward shortwave radiation</td><td>$W.m^{-2}$</td><td rowspan="2">CORE
daily
climatology
1.875°</td><td colspan="2" rowspan="2">CORE
daily
1.875°</td><td rowspan="2">ISCCP*
daily
climatology
1.875°</td><td colspan="2" rowspan="2">ISCCP*
daily
1.875°</td><td rowspan="2">ISCCP*
daily
climatology
1.875°</td><td rowspan="2">ISCCP*
daily
1.875°</td><td rowspan="4">ERAi**
daily
1.125°</td></tr>
<tr><td>radlw</td><td>Downward longwave radiation</td><td>$W.m^{-2}$</td></tr>
<tr><td>P</td><td>Total precipitation</td><td>mm/day</td><td rowspan="2">CORE
monthly
climatology
1.875°</td><td colspan="2" rowspan="2">CORE
monthly
1.875°</td><td rowspan="2">GXGXS*
monthly
climatology
1.875°</td><td colspan="2" rowspan="2">GXGXS*
monthly
1.875°</td><td rowspan="2">GXGXS*
monthly
climatology
1.875°</td><td rowspan="2">GXGXS*
monthly
1.875°</td></tr>
<tr><td>snow</td><td>Snow fall</td><td>mm/day</td></tr>
</table>

* *: With corrections as described in Brodeau et al. (2010) to reduce time discontinuities when matching different data sets and to reach a nearly closed global balance.*

** *: ERAi 6 hourly residues (calculated as the difference between instantaneous original ERAi fields and the ERAi daily mean climatology of the period 1979-2001) are added to the climatological daily mean (period 1979-2001) of DFS4.4.*

9 ACKNOWLEDGEMENTS

The authors were supported by Centre National de la Recherche Scientifique (CNRS) and Université de Grenoble-Alpes (UGA). This work is a contribution to the DRAKKAR GDRI which acknowledges the support of CNRS and IFREMER. It was granted access to HPC resources under the allocations x2013-010727 and x2014-010727 attributed by GENCI to DRAKKAR, simulations being carried out at both the IDRIS and CINES supercomputer national facilities. Research leading to these results also benefited from some support provided by: the programme LEFE/GMMC to DRAKKAR: the Centre National d'Etudes Spatiales (CNES) and: the FP7 MyOcean Project.

10 REFERENCES

Brodeau et al., 2012. An ERA40-based atmospheric forcing for global ocean circulation models. Ocean Modelling, Volume 31, Issues 34, 2010, Pages 88-104, ISSN 1463-5003

Dee et al., 2011. The ERA-Interim reanalysis: configuration and performance of the data assimilation system. Quart. J. R. Meteorol. Soc., Volume 137, Pages 553-597.

Hurrell, J.W., Hack, J.J., Shea, D., Caron, J.M., Rosinski, J., 2008. A new sea surface temperature and sea ice boundary dataset for the community atmosphere model. J. Clim. 21 (19), 5145–5153.

Josey S. A., L. Yu, S. Gulev, X. Jin, N. Tilinina, B. Barnier, L. Brodeau, 2014: Unexpected impacts of the Tropical Pacific array on reanalysis surface meteorology and heat fluxes. Geophys. Res. Letters, Vol: 41, DOI: 10.1002/2014GL061302.

Large, W.G., Yeager, S.G., 2004. Diurnal to decadal global forcing for ocean and sea-ice models. NCAR Technical Note, p. 22.

Mathiot, P., B. Barnier, H. Gallée, J.-M. Molines, J. Le Sommer, M. Juza, and T. Penduff, 2010: Introducing katabatic winds in global ERA40 fields to simulate their impact on the Southern Ocean and sea-ice. *Ocean Modelling*, 35(2010)146–160.

Meinvielle M., J.-M. Brankart, P. Brasseur, B. Barnier, R. Dussin, and J. Verron, 2013: Optimal adjustment of the atmospheric forcing parameters of ocean models using sea surface temperature data assimilation. Ocean Science, ç, 867-883. doi: 10.5194/os-9-867-2013.

Pinker R.T. and I. Laszlo, 1992: Modeling Surface Solar Irradiance for Satellite Applications on a Global Scale, J. Appl. Met., 31, 194-211).

Rigor, I., Colony, R., Martin, S., 2000. Variations in surface air temperature observations in the Arctic. J. Clim. 13, 896–914.

Storto A., I. Russo , and S. Masina, 2013. Interannual response of global ocean hindcasts to a satellite-based correction of precipitation fluxes. Personnal communication.

Zhang, Y.C., Rossow, W.B., Lacis, A.A., Oinas, V., Mishchenko, M.I., 2004. Calculation of radiative fluxes from the surface to top of atmosphere based on ISCCP and other global data sets: refinements of the radiative transfer model and the input data. J. Geophys. Res. 109, 27.